EVOLUTION OF EXPERIMENTAL AND NATURAL RIVER BASINS IN VIEW OF THE PACHMARHI

Dr. N.L. Dongre.

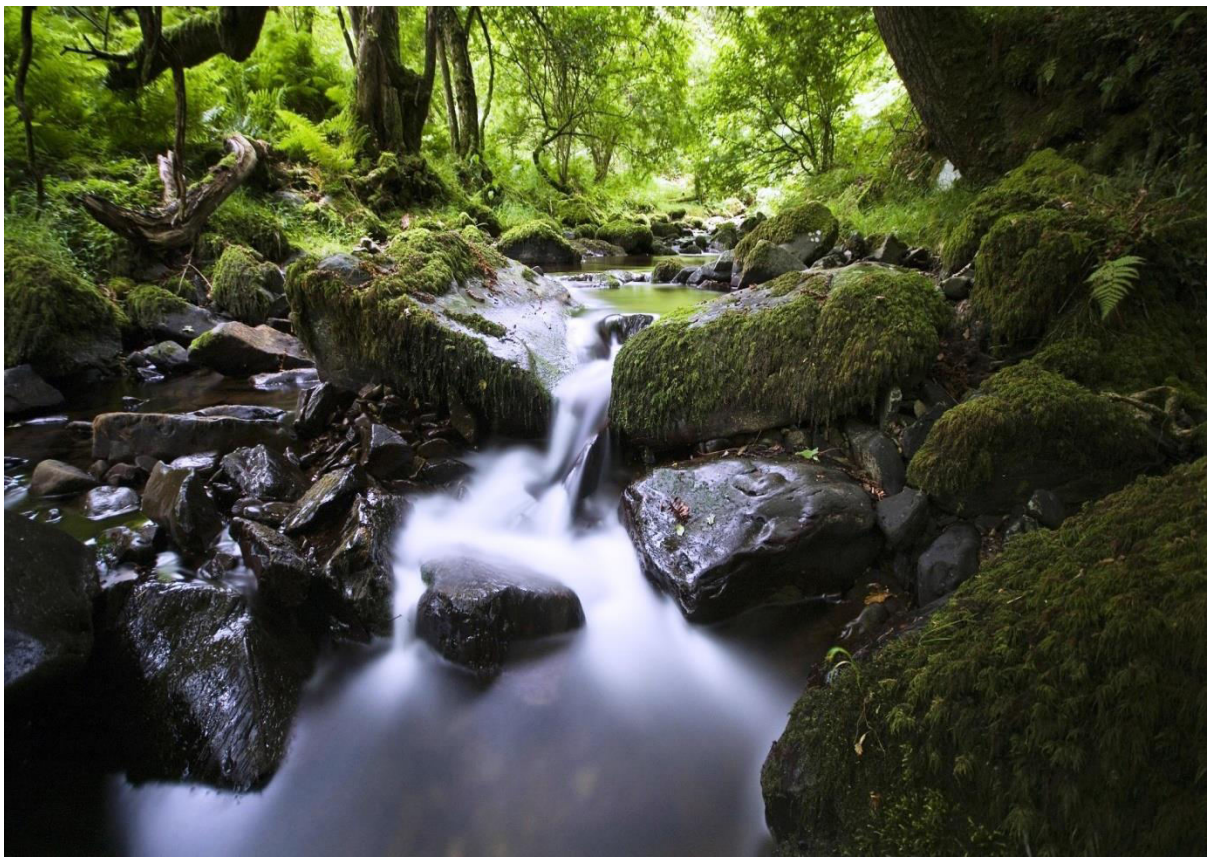

The growth of relief in active tectonic areas of Pathalkot of the Pachmarhi (India) is mainly controls by the interaction between tectonic and surface processes. The study of long-lived morphologic markers formed by these interactions can help in quantifying the competing effects of tectonics. This regions experiencing active extension of the Dudhi river-long profiles and faceted spurs can help in understanding the development of mountainous topography along normal fault scarps. In this study it is developed analogue experiments that simulate the morphologic evolution of a mountain range bounded by a normal fault. The analysis of the modelled catchments allows comparing with a natural case.

ABSTRACT [1] *Several quantitative models have been developed to simulate the long-term evolution of river basin topography. Many of these models reach an equilibrium state when the base level is lowered at a constant rate and the substrate and climate are constant in time. At the equilibrium, erosion balances the base level lowering, causing topography remains frozen in time. But, some recent laboratory experiments contradict this behavior. In present experiments the space-time mean erosion rate balances the base level lowering rate, but the actual erosion rates are highly variable in space and time. Consequently, the channel networks are substantially mobile. The experimental flow conditions are approximately similar but not dynamically equivalent to those in nature, so it is unclear whether the observed dynamics are representative. This article examines whether the processes occurring in the experiments produce basins that are geometrically similar to typical natural basins of the Pachmarhi. To make this evolution, the conceptual framework of scaling invariance is used. Various similarities are observed, but it is found that the experimental basins are slightly more elongated across a range of scales than the natural basins are considered and the relationship between channel slope and drainage area exhibits a break that is not found in the natural basins. In the experiments the slopes of small channels also depend on the proximity of large channels. This dependency is more pronounced for experiments with more mobile channel networks, and it is not observed in most of the analyzed natural basins.*

Keywords: Laboratory experiments, drainage basin, force budget, Knick point

1. Introduction

[2] Laboratory experiments in long-term drainage basin evolution offer an extraordinary opportunity to explore Landscape behavior under a variety of conditions in the Pachmarhi. Rainfall intensity, substrate characteristics, deformation mechanisms, and base level movement can all be controlled, and the resulting behavior of the drainage basins can be observed. Such experiments allow researchers to visualize the behavior of drainage basins under specific conditions and to test theoretical models of geomorphic processes. While several small experimental studies have been reported in the recent past, this approach has been largely underutilized due in part to technological constraints. However, advances in computing and monitoring devices now allow highly detailed measurements to be made in both space and time. One can document the form of the topography, the rates of erosion, the occurrence of discrete events (such as hillslope failures and knickpoint propagation), and the systematic interactions of processes.

[3] Results from physical experiments have offered important insights into the dynamics of eroding drainage basins, particularly with respect to intrinsically driven instabilities. For example, *Schumm and Parker* [1973] and *Parker* [1977] observed a complex response where fluvial incision triggers hillslope failures, which stymie further incision until channels have excavated the excess sediment supplied from the failures. *Hasbargen and Paola* [2000, 2003] observed unexpected instabilities as well. They examined the behavior of drainage basins when the rainfall and substrate properties are constant in space and time and the base level is lowered at a constant rate. After a period of time, the topography evolves to a flux steady state where the space-time mean erosion rate balances the base level lowering rate, but the erosion rate at a given location and time varies stochastically. This behavior induces divide migration and drainage network rearrangement over timescales that correspond to the erosion through a significant fraction of total basin relief. The observed behavior at the flux steady state is not expected from numerical landscape evolution models *[Willgoose et al.,* 1991a; *Howard,* 1994; *Moglen and Bras,* 1995a]. Both detachment-limited and transport-limited models *[Howardet al.,* 1994; *Paola,et al* 2009] suggest that the topography becomes frozen in time when the climate and substrate characteristics are constant and the base level is lowered at a constant rate. Such models produce stochastic flux steady state behavior only when randomness is imposed externally [e.g., *Ellis etal.,* 1999].

[4] It is clear that small and simplified physical experiments are not exact models for larger and more complicated natural basins. The experiments do incorporate mass transport processes that resemble landscape-scale processes (namely erosion by surface runoff), and the simulated basins exhibit visual similarity to real basins. However, exact dynamic similarity is not possible, so the relative magnitudes of forces in the experiments are different from those in real basins (it is discussed this in greater detail later in the paper). Thus the degree to which physical experiments represent the long-term evolutionary processes of natural basins remains unclear. Is the difference in dynamic scaling important to the evolutionary dynamics? Are the unexpected instabilities and dynamics exposed by quantitative measures of basin morphology?

[5] In this paper a step is taken by us towards answering these questions. It is compared that the morphology of experimental and natural basins to determine whether the simulated basins quantitatively resemble natural basins, and the results are compared from different experimental conditions to determine whether the amount of network reorganization and divide migration is evident in the associated landscape morphology. The framework of scaling invariance is used to make these comparisons. Scaling invariance is a widely observed and relatively well-quantified property of natural basins *[Peckham,* 1995; *Maritan et al.,* 1996; *Rodriguez-Iturbe andRinaldo*, 1997; *Veneziano and Niemann,* 2000a; *Dodds and Rothman,* 2001]. Thus it provides a suitable tool to characterize the experimental topographies. In this paper, it is focused on four properties of basins and how they change across scales. These properties are: the horizontal shapes of basins, the sinuosity of the mainstreams, the relationship between channel slope and drainage area, and the variability of channel slope for a given drainage area. Section 2 begins with an overview of published experiments with small drainage basins, and section 3 follows with a discussion of the experimental setup and flow conditions. Section 4 presents the morphological comparison of natural and experimental basins, and section 5 closes with the conclusions.

2. Background

[6] This section provides a brief review of published laboratory experiments involving erosion in small drainage basins. Although each of these experiments focused on certain aspects of landscape evolution and morphology, the common process of runoff-based erosion is repeated in all of them. Here, it is specifically examined that the robustness of the drainage forming process over a broad range of experimental conditions.

[7] *Parker* [1977] employed a rectangular flume (9.1 m × 15.2 m × 1.8 m) with a single outlet, and applied rainfall rates of 5.8×10^{-6} to 18.4×10^{-6} m/s (droplet size~1.5×10^{-6} m) over a substrate composed of silt/clay particles mixed with sand ($D_{50} = 3.75 \times 10^{-3}$ m). These experiments studied drainage planform evolution after a stepwise lowering of the base level. A decline in drainage density was observed after the network had completely extended to the edges of the basin. Knickpoints were observed in the streams as transient features that sometimes disappeared and sometimes coalesced to form larger knickpoints. Eroded material from knickpoint propagation was often deposited just downstream of the migrating knickpoint. Cyclical sediment yields were observed at the outlet following the stepwise base level drop and were considered a result of sediment storage associated with out-of-phase erosion of the hillslopes and streams (i.e., complex response *[Schumm and Parker,* 1973; *Parker,* 1977]).

[8] *Czirok et al.* [1993] explored the evolution of topography by sprinkling rainfall over a smoothed 0.65 m linear ridge of silica sand ($D_{50} = 1.5 \times 10^{-4}$ m) mixed approximately 1:1 with organic soil. In these experiments, erosional processes included landslides of widely varying sizes and entrainment of particles by surface runoff. Surface roughness compared favorably to the Planet Mars and its drainage basin. Suggested that the fractal character of mountainous landscapes was due to surface runoff and the presence of landslides over a range of scales.

[9] *Ouchi and Matsushita* [1992] constructed a similar test to *Czirok et al.* [1993]. These experiments focused on the evolution of relief. The experimental setup consisted of a 1 m by 1 m table loaded with a 0.2 m block of sediment ($D_{50} = 0.12 \times 10^{-4}$ m; mixed 15:1 by weight with kaolinite). Rainfall was applied at a rate of 7×10^{-6} to 14×10^{-4} m/s for 192 hours, and topographic profiles were measured with a point gauge at nine times during the run. *Ouchi and Matsushita* [1992] documented the initial dissection of the original plateau, with an increase in roughness, followed by an exponential decay of the relief.

[10] *Hancock* [1997] developed an erosion facility (1.44 m ×1.46 m × 0.5 m) to explicitly test a numerical landscape evolution model *[Willgoose et al.,* 1991a]. These experiments focused on calibrating the model parameters and comparing the spatial statistics of the experiments with numerical simulations. In these experiments, a stepwise drop in base level at the tank outlet simulated block uplift, similar to *Parker's* [1977] experiments. Rainfall rates were varied from 8×10^{-6} to 33×10^{-6} m/s, with droplet size less than 270×10^{-6} m. The substrate consisted of fly ash, a byproduct of coal combustion ($D_{50} = 81 \times 10^{-6}$ m). While the qualitative form of the experimental basins differed substantially from the numerical model of *Willgoose et al.* [1991a], certain spatial statistics such as the distribution of cumulative area draining through a point and hypsometry compared moderately well. The experiments produced a power law relationship between the channel slope S and the associated drainage area $A\left(S \propto A^{-\theta}\right)$ where $\boldsymbol{\theta}$ ranged from 0.02 to 0.27 *[Hancock,* 1997].

[11] Recently, several researchers have developed physical experiments that forced the landscape with continuous uplift and rainfall conditions *[Hasbargen and Paola,* 1998; *Hasbargen and Paola,* 2000; *Crave et al.,* 2000; *Ouchi,* 2002; *Lague et al.,* 2003; *Hasbargen and Paola,* 2003]. The erosion facility of *Crave et al.* [2000] and *Lague et al.* [2003] consisted of a small rectangular box (0.2 m × 0.3 m × 0.09 m) containing loess ($D_{50} = 50 \times 10^{-6}$ m, consisting of 10% clay, 10% $CaCO_3$, 80% silt)

Table 1. Characteristics of the Experiments Analyzed in This Study[a]

Experiment	Base Level Lowering Rate, m/s	Rainfall Rate, m/s	Mean Relief in Flux Steady State, m
2	2.82×10^{-6}	3.86×10^{-6}	0.286
4	0.55×10^{-6}	6.2×10^{-6}	0.176
5	1.47×10^{-6}	16.3×10^{-6}	0.170
6	0.94×10^{-6}	13.5×10^{-6}	0.158

[a] In all experiments the tank area was 6250 cm^2, and the substrate was crushed silica flour ($D_{50} = 45 \times 10^{-6}$ m) mixed with 1% kaolinite by weight. Experiments were conducted at Jaypee laboratory, Rewa,

India in October 2003 (experiment 2), September 2014 (experiment 4), May 2015 (experiment 5), and July 2015 (experiment 6). Experiments were observed on the basis of literature available in article of – Hasbargen (2005)

with a rainfall generating device above the facility. The rainfall rate was 25 $\times 10^{-6}$ m/s and the droplet size was 8 $\times 10^{-6}$ m. Sediment and water exited the box along its edges. Uplift rates of 2.8 $\times 10^{-6}$ to 28 $\times 10^{-6}$ m/s were accomplished by pushing the box past fixed borders using a motor-controlled infinite screw device. This setup was used to document the dissection of an initial plateau under constant uplift followed by decline in relief upon termination of uplift. Using gridded elevation data, the slope and drainage area were found to be weakly related, with $\boldsymbol{\theta} \approx 0.1$. *Lague et al.* [2003] noted that this value is close to the one observed for natural colluvial channels and unchanneled valleys in the Siwalik Hills of India ($\boldsymbol{\theta} \approx 0.18$), but it is lower than values commonly observed for natural alluvial rivers ($0.3 \leq \boldsymbol{\theta} \leq 0.8$) *[Lague et al.,* 2000] and badlands ($\boldsymbol{\theta} \approx 0.19$) *[Howard and Kerby,* 1983]. These experiments were too small for dendritic drainage patterns to develop, so the results are analogous to low-order channels and hillslopes *[Lague et al.,* 2003].

[12] Together these results demonstrate that experimental drainage basins can develop in a variety of substrates (grain sizes ranging from 50 $\times 10^{-6}$ to 3750 $\times 10^{-6}$ m, with varying concentrations of sand and clay) and under a wide range in rainfall conditions (2.8 $\times 10^{-6}$ to 33 $\times 10^{-6}$ m/s with droplet sizes from 8 $\times 10^{-6}$ to 3710 $\times 10^{-6}$ m). The horizontal areas of the experimental landscapes also varied by several orders of magnitude from 0.06 to 138 m^2, and dendritic channel networks of at least order 5 have been documented *[Hancock,* 1997; *Hasbargen and Paola,* 2000]. Furthermore, these experiments all share a common mechanism for removing sediment from the landscape: erosion by surface runoff.

3. Experimental Design

3.1. Experimental Apparatus and Run Conditions

[13] This experimental setup was based on experiments observed by *Hasbargen,* 2005, consisted of a rigid metal tank with a single outlet. The planform of the tank was elliptical, with a long axis of 0.99 m and short axis of 0.87 m. The tank depth was 1.0 m. The outlet elevation was controlled by a motor, capable of dropping the outlet at a very slow rate, on the order of 10^{-6} m/s. A mist apparatus supplied the rainfall. The droplet size was small enough ($<10^{-4}$ m) that the impacts did not displace surface material. The substrate consisted of silica flour (D_{50} = 45 $\times 10^{-6}$ m) mixed in a cement mixer with water and 1% (by weight) kaolinite to provide cohesion. This mixture was poured into the basin and allowed to settle overnight. The initial topography produced by this procedure was nearly flat.

[14] In this paper, data is presented from the flux steady state of four separate runs that were conducted at varying rainfall and base level lowering rates (see Table 1 for run conditions). Both the rainfall and base level lowering rates were varied by a factor of about four between runs (3.9 $\times 10^{-6}$ to 16.3 $\times 10^{-6}$ m/s, and 0.55 $\times 10^{-6}$ to2.8 $\times 10^{-6}$ m/s, respectively). Each run was conducted under continuous base level fall and rainfall conditions except for short interruptions in rainfall for time lapse video collection (approximately 10 s interruptions every 300 s) and digital stereo photograph collection (approximately 10 min interruptions every several hours). The size of the tank was sufficient for third- to fifth-order drainage basins to develop (Figure 1), and the tank depth allowed the basins to erode through a depth of 1 to 4 times the instantaneous relief after complete dissection of the initial surface. Surface runoff caused most of the erosion, but local slumping of hillslopes occurred in some of the runs. The ratio of the rainfall rate to the base level lowering rate dictated erosional process activity in our experiments. For lower values of this ratio (experiment 2), hillslope failures were more common and the relief was higher. For higher values of this ratio (experiments 4, 5, and 6), the erosion related to surface runoff was more important, and the relief was lower. Measurements of sediment flux at the outlet indicated that a steady state was reached where the mean erosional flux balanced the input from the uplift relative to the base level. This flux steady state occurred shortly after dissection of the initial flatsurface. As described earlier, the local erosion rate during the flux steady state varied stochastically in time. In all of the runs presented here, knickpoints developed and propagated upstream and the channel networks exhibited a tendency to migrate and reorganize *[Hasbargen and Paola,* 2000, 2003]. This behavior was most significant in experiments 2 and 6.

3.2. Evaluation of Dynamic Similarity

[15] Ultimately, physical experiments are conducted to replicate the relative importance of the various forces at work in natural basins. However, it is not possible to obtain exact dynamic similitude between natural rivers and channels in a flume. In this section, it is demonstrated that breakdown in exact dynamic similitude, but it is also shown that experimental basins can develop flow dynamics, characterized by the Froude number, that approximate those in much larger natural drainage basins.

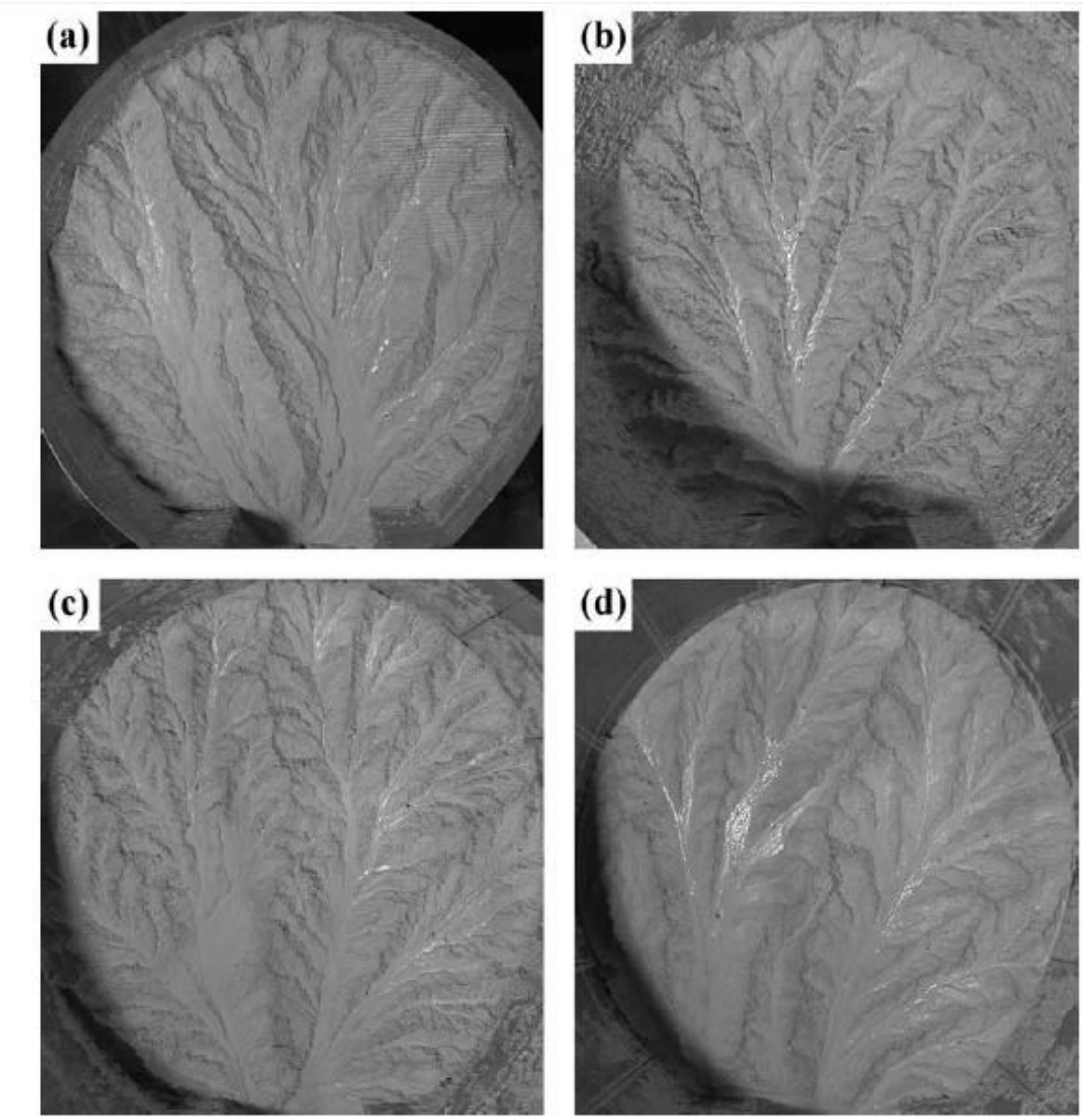

Figure 1. Photographs taken of the basins developed in the four experiments. Figures 1a-1d correspond to experiments 2, 4, 5, and 6, respectively.

$$\frac{\partial U}{\partial t} + U\frac{\partial U}{\partial x} + V\frac{\partial U}{\partial y} + W\frac{\partial U}{\partial y} = -\frac{1}{\rho}\frac{\partial P}{\partial x}$$

[16] It is started with an overview of the forces operating in fluid flow as encapsulated by the Navier-Stokes equation. The Navier-Stokes equation can be written in the *x* direction, which is defined as the downstream direction, as

$$+v\left(\frac{\partial^2 U}{\partial x^2} + \frac{\partial^2 U}{\partial y^2} + \frac{\partial^2 U}{\partial z^2}\right) + \mathrm{g}x \tag{1}$$

where *U, V,* and *W* are the velocity components in the *x, y,* and *z* directions, ρ is the density of the fluid, v is the kinematic viscosity (dynamic viscosity divided by fluid density), *P* is the pressure, and g_x is the component of gravity in the *x* direction. The first term on the left side is the temporal acceleration and the next three terms represent spatial accelerations. The terms on the right side correspond to pressure, viscous, and gravitational forces, respectively. To get a sense of the relative importance of the terms in equation (1), the differential terms can be replaced with their dimensions,

and each term can be divided by the dimensions of the spatial acceleration terms, which are the terms typically known the least about. Doing this, it is obtained

$$\frac{U/t}{U^2/L} + \frac{U^2/L}{U^2/L} = \frac{P/(L\rho)}{U^2/L} + \frac{\nu U/L^2}{U^2/L} + \frac{g_x}{U^2/L}. \quad (2)$$

After simplifying and rearranging, this equation becomes

$$1 = \frac{P}{U^2\rho} + \frac{\nu}{UL} + \frac{g_x L}{U^2} - \frac{L}{Ut}. \quad (3)$$

If it is assumed steady flow, then the temporal acceleration term $L/(Ut)$ can be neglected. If it is also assumed uniform flow with no pressure gradient in the streamwise direction, then the pressure term $P/(U^2\rho)$ can be neglected. Thus, for steady uniform flow, it is obtained

$$1 = \frac{\nu}{UL} + \frac{g_x L}{U^2}. \quad (4)$$

Notice that

$$R_e \equiv UD/\nu$$

$$F_r \equiv U/(gD)^{1/2} \quad (5)$$

where R_e is Reynolds number, F_r is Froude number, D is flow depth (the appropriate length scale), and g is gravity. Equation (4) implies that the dynamics of the flow are described by the Reynolds and Froude numbers. The Reynolds number compares advective acceleration to frictional resistance (viscous forces) and discriminates between laminar (R_e < 500) and turbulent (R_e > 500) flow conditions. The Froude number compares advective to gravitational accelerations and characterizes flow conditions as subcritical (or tranquil) (F_r< 1), critical (F_r =1), or supercritical (or shooting) (F_r > 1) (see *Peakall et al.* [1996] for a similar scaling argument).

[17] These two numbers offer a direct method of establishing dynamic equivalence. In order for the experiment to be dynamically similar to a natural system, it must have the same R_e and F_r as the natural system. If g and ν are considered to be constant between natural and experimental channels, dynamic similarity requires

$$\frac{U_e D_e}{\nu} = \frac{U_n D_n}{\nu} \quad (6)$$

and

$$\frac{U_e}{(gD_e)^{1/2}} = \frac{U_n}{(gD_n)^{1/2}} \quad (7)$$

where the subscripts *e* and *n* denote the experimental and natural channels, respectively. Thus, for any set flow conditions characterized by given R_e and F_r numbers, there are two equations and two unknowns (U_e and D_e), which implies uniqueness. This presents a problem for dynamically scaled modeling. If one chooses a smaller depth for the experimental channel than the natural channel, say by a factor of 10, then the velocity would need to increase by a factor of 10 to satisfy equation (6) and by a factor of 10 to satisfy equation (7). These conflicting requirements imply that dynamic similitude cannot be maintained without changes in either gravity or kinematic viscosity. Unfortunately, the required increase in gravity is not easy to achieve in a flume, and the only fluids available with the required viscosity are toxic. Thus dynamic equivalence is not possible in practice, and the relative magnitude of the forces acting in the experiment is expected to differ from those in nature significant role in the drainage system.

[18]. Many questions have been addressed about the possible couplings between experimental and tectonically controlled natural rivers. To get result of comparison, drainage basin of four rivers of the Pachmarhi, India is analized. These rivers- Denwa, Bainganga, Dudhi and Nagduari are playing significant role in the drainage system (figure; 2a and b). This analysis led to a considerable improvement in the mathematical modelling of surface process, in particular with the advent of experimental and numerical models of landscape and drainage evolution and with the quantitative analysis of increasingly available high-resolution datasets of the Earth's topography. How different are the flow conditions in the experiments from those in natural rivers? For natural channels, tranquil

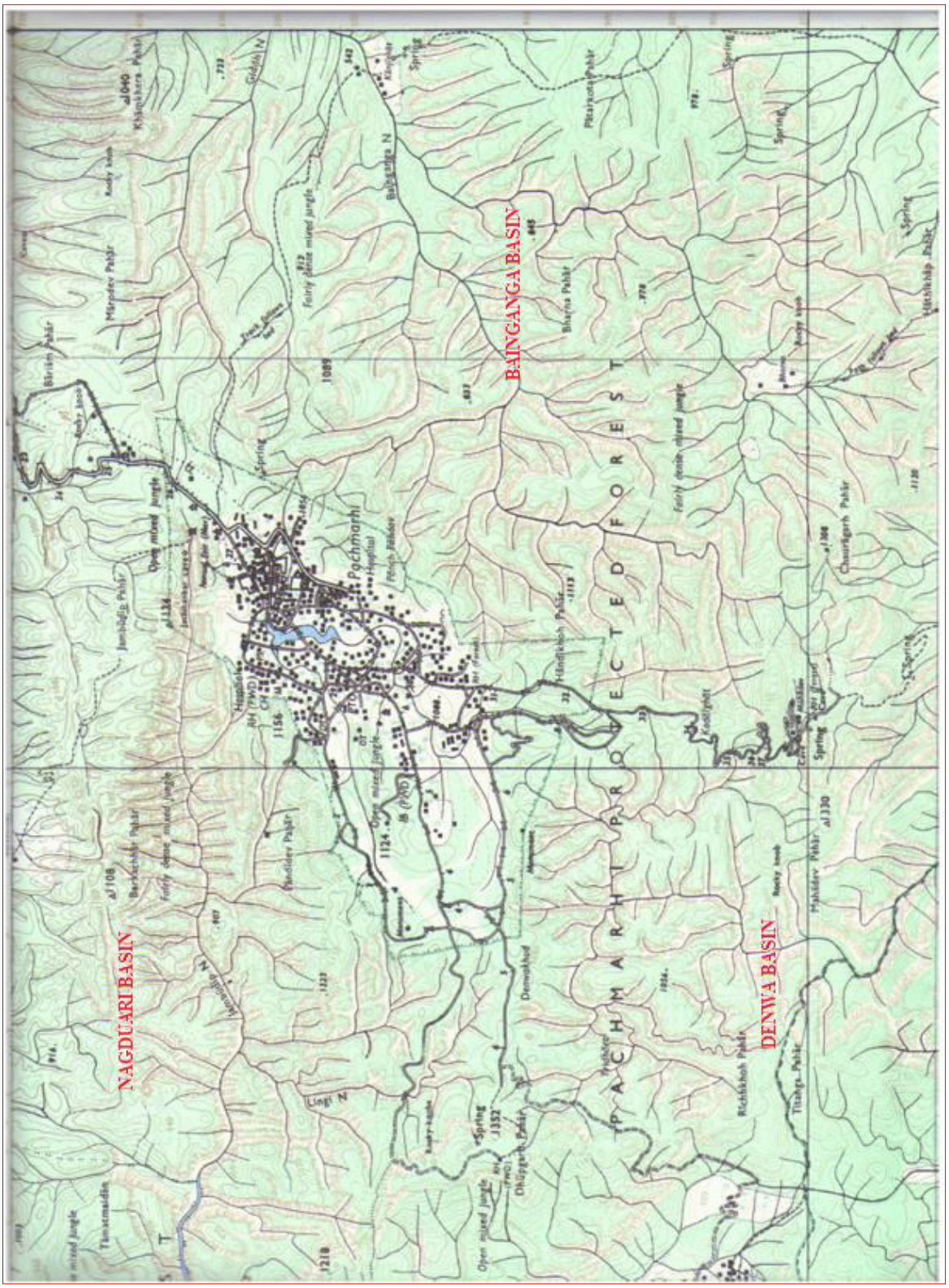

Figure. 2a, Survey of India toposheet – 55, J/7. The descriptive morphology of visible Denwa basin, Bainganga basin and Nagduari basin networks has been used to argue for or against particular processes responsible for the observed structures. It is submitted that drainage basins, extracted from topography, are more objective means to address this question, because they pertain to the overall roughness of the landscape rather than to its individual features. In particular, the landscape erosion caused by a sustained rainfall would imprint a characteristic drainage pattern on the Denwa, Bainganga and Nagduari basin surface that should be recognizable by means of a network descriptor, even if prominent features such as sapping-induced valley networks and impact are interwoven into the original landscape.

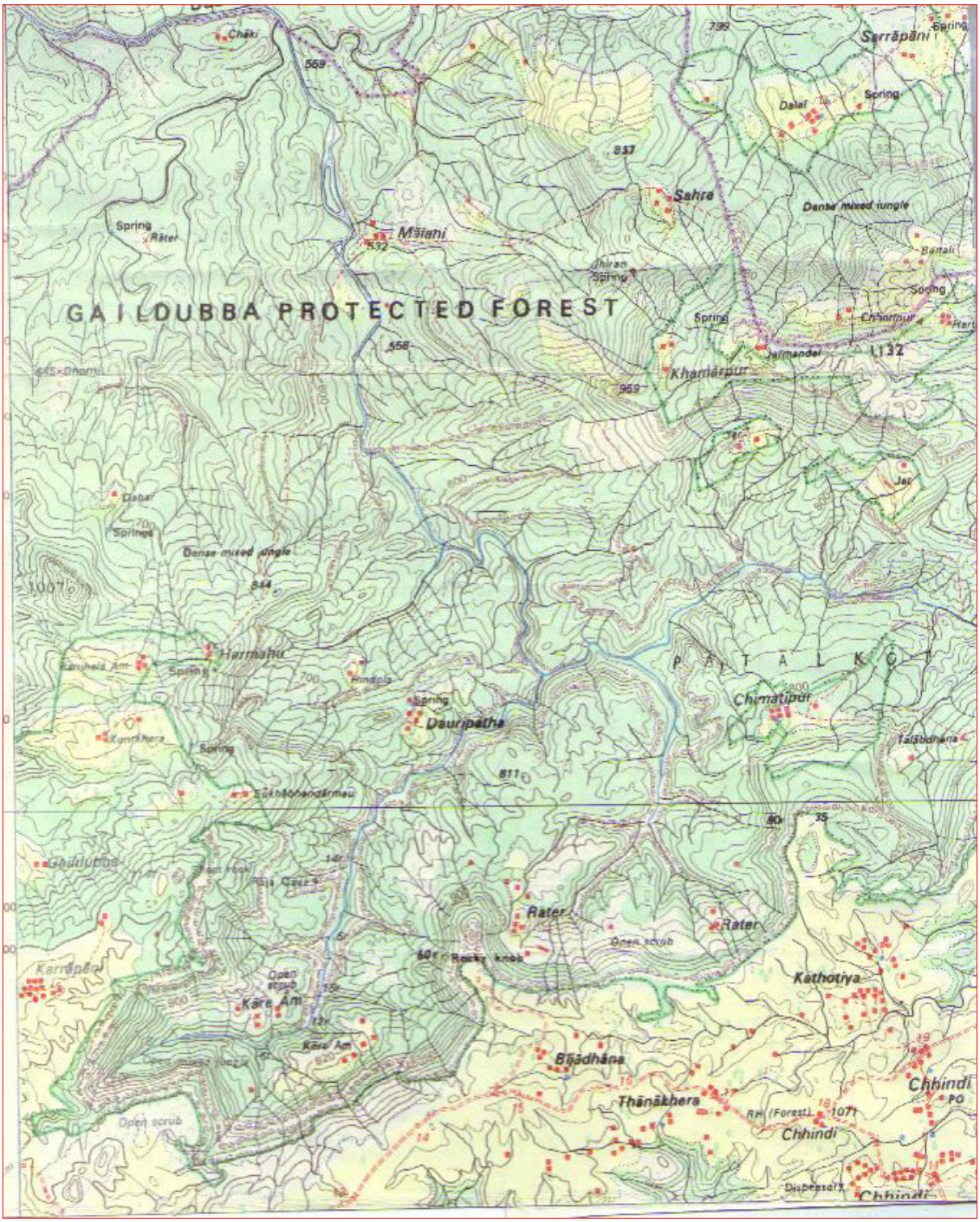

Figure.2b. A, Survey of India toposheet – 55, J/15 Investigations concerning the relationship of stream flow orientation with geological structure in the Dudhi Basin shows that, generally, the least influenced flows are those of first order; less influenced are the first order streams which are governed simply by the valley side slopes on which they developed. However, in certain geological and geomorphologic situations, there are clear exceptions to this generalisation; certainly, locally, geological control of these small streams may be even higher than in many streams of higher order. In the peripheral parts of the basin, expansion of drainage into the available space has obviously been easiest along lines of weakness and, as a consequence of this, streams of the first order come to exhibit a high degree of adjustment to the underlying structure.

flows are Common, but steepened reaches may have critical or shooting flows. Open channel flows are generally turbulent, but very shallow flows on smooth hillslopes may be laminar. To get a rough idea of flow conditions in the basins it is analyzed later and obtained measurements from Tawa gauging stations on the Tawa river in India , which is the closest gauging station to the Denwa, Bainganga, Dudhi and Nagduari basin and drains an area of similar size to the Tapti basin. These basins are described in more detail in section 4. From velocity and depth measurements, Reynolds numbers range from 10,700 to 1,200,000 at the gauging station.Froude numbers range from 0.03 to 0.12 for the Denwa and from 0.01 to 0.54 for the Bainganga. Thus gravity is the most important term in the force budgets of these rivers, with inertial forces (velocity changes) playing a less significant role. Viscous forces are much less important than both gravitational and inertial forces. Note that these results pertain only to the gauging station locations.

[19] For the experiments, the shallowest flows occur on the hillslopes, where flow depths are —10~^{4} m and velocities are —10~^{3} m/s. Using a kinematic viscosity of 10~^{6} m^{2}/s for pure water, these values imply laminar flow with R_e ~ 0.1 and tranquil flow with F_r — 0.03. Hence, at very small scales, viscous and gravity forces dominate the force budget, with inertial (that is, spatial accelerations) playing a lesser role. A maximum *Re* can be determined by considering the flow at the tank outlet, which is constricted to a width *W* of 10~^{2} m. Among all the experiments presented here, the maximum discharge *Q* at the tank outlet is —10 mL/s. The product *UD* in the Reynolds number can be found by *Q/W,* and the resulting *Re* is —1000, which implies turbulent flow. A maximum *Fr* can be determined by considering the channels just upstream from the outlet. The depth is about —10 ~^{3} m and the velocity is about —10~ m/s, which yields F_r — 1 or approximately critical flow. In addition, it is observed that small standing wave trains in experimental channels diagnostic of critical and shooting flow.

[20] To summarize, the experimental flow conditions have Froude and Reynolds numbers that span the following ranges: $0.03 < F_r \leq 1$ and $0.1 < R_e < 1000$. Thus Froude numbers for the experiments are similar to those observed in natural basins, but Reynolds numbers are much lower for the experiments than for the natural flows. In both natural and experimental cases, however, the gravitational and inertial forces dominate the force budget in the channels, and in this sense the experimental flows resemble natural flows. It is interesting to note that numerous experiments have produced visually realistic dendritic channel patterns despite Reynolds numbers that deviate from those in natural systems and sometimes indicate laminar flow. This observation suggests that turbulence is not required for the development of convergent flow networks.

3.3. DEM Extraction and Processing

[21] In order to characterize the experimental topography, digital stereo photographs (taken by a 1280 × 960 pixel resolution Nikon Cool Pix 900) were used to develop gridded elevation models. The process involved several steps. First, the locations of the camera and benchmarks on the basin walls were measured in an arbitrary fixed ground reference frame. Then, the coordinates of the benchmarks were collected for each photograph, and corresponding points in the stereo photographs were automatically identified and extracted using a pixel gray value cross correlation search algorithm. Camera orientations and effective focal lengths were then computed by solving the co linearity equations, utilizing known camera locations and control points on the ground [see *Wolf,* 1983, Appendix C]. Once the camera orientation parameters were determined, the ground coordinates of corresponding photographic point pairs were computed by solving the co linearity equations for the ground coordinates. These *x*-*y*-*z* coordinates were then read into a grid at 5 mm spacing, and missing data points were determined by interpolation. The precision of photogrammetric solutions using a 1280 × 960 pixel resolution camera is modest. Each pixel corresponds to a 0.4 mm length on the ground, and the vertical resolution from the procedure ranges from 7 to 20 mm, depending on the field of view and the distance between the ground surface and camera. The coarse resolution in the vertical direction produces some step-like artifacts in the elevation model. Furthermore, some faulty correlations result from the automated image correlation process, which introduces some unrealistic roughness. To confront these two artifacts, locations with slopes greater than 2 or less than 0.001 were identified, and the elevations at those points were replaced by local averages. This procedure removed the unrealistic noise without excessively smoothing the surface.

4. Morphological Evaluation

[22] No dimensional measures of river basin morphology provide a convenient framework to quantitatively compare topographies generated in a laboratory setting with those observed in nature. In this section, scaling-invariance conditions are used that have been observed for natural river basin topography to derive no dimensional measures of topography. It is then applied that these measures to characterize the experimental and natural basins. The experimental landscapes analyzed herein are

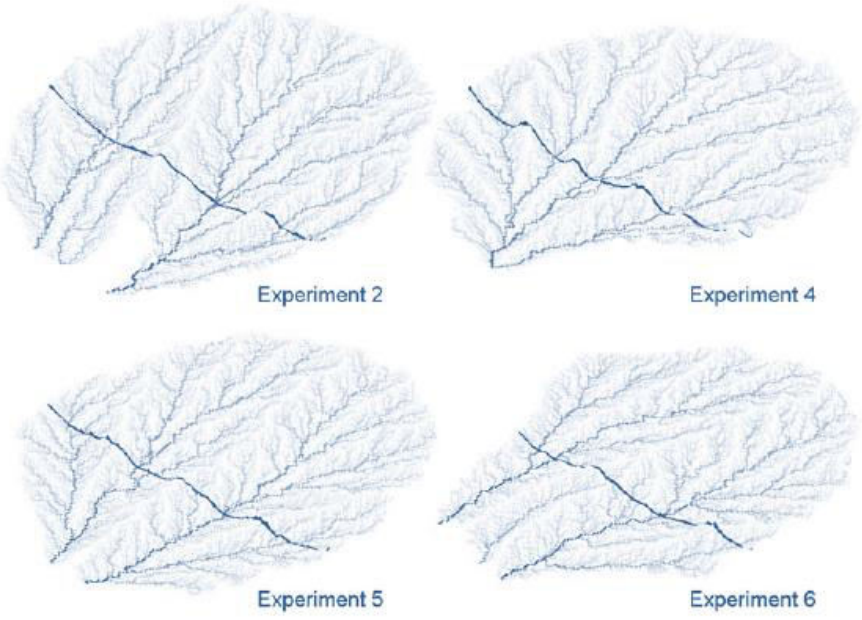

Figure 3. Three-dimensional renderings of the experimental basins analyzed in this paper. The shading is determined from the drainage areas, except for the black transects, which highlight the shapes of the main valleys.

eroding at a flux steady state, where on average the erosional flux balances uplift. For the purpose of brevity, the discussion focuses on only one topography from each of the experiments described in Table 1 (experiments 2, 4, 5, and 6). These topographies were selected using two criteria: (1) they have few artifacts from the data processing procedures, and (2) they are morphologically typical for their respective experiments. Figure.3 shows the four experimental topographies with shading according to drainage area. Visual inspection suggests that the topographies are generally realistic with irregular, aggregating valley patterns extending throughout the tank.

[23] For comparison it is analyzed a series of natural drainage basins as digital elevation models. These basins were selected in part because they have typical basins characteristics. They have clear, possible influence of geological structure on stream flow direction is best studied in basins where there is an absence of weathering mantles and sedimentary fills, and in these respects, the Pachmaris drainage basins are an important and ideal. The aim of this paper is to determine to what extent is this consequent course of the river basin to facilitate comparison between natural and experimentally generated river basin 4 basins are extracted from the Pachmarhi. The first is the Denwa basin, second the Bainganga basin, third is the Dudhi basin and Nagduari is fourth one (Figure:2-a and b**,)** ha**ve** been affected by the underlying rock structure. The analysis was conducted at a local or meso-scale as defined by the degree to which streamflow direction has adjusted to fault traces, mylonite zones, thrust fronts and lineations of the crystalline basement of experimental and natural structure. The bedrock**s** of the Pachmarhi comprise basalt and sandstone rocks which are transected by a dense network of fractures. The component rocks are disposed in sub-parallel bands and lenses which vary in width from 100 to 1000 m; Such a spatial configuration of structural detail is unique to the Pachmarhi. The major part**s** of the basin**s** are floored by the sandstone and deccan trap rocks. The original southerly streamflow of the area is presumably indicated by the direction of the upper reaches. Extensive phenomenological studies of this drainage (river) networks showed that their geometrical and topological structure is charectarised of drainage network is corroborated by several network quantities. The drainage network was derived from topographic maps at a scale of 1:50,000. Both perennial and ephemeral streams were included. The network was then divided into segments, i.e. reaches between the source and a confluence or reaches between confluences. For each segment, the orientation and rectified length were determined. Measurements of structural elements were made from geological maps. Lineations were grouped into twelve 15° intervals. The preferred stream-flows were determined from the knowledge of the orientation and relative length of drainage elements and then compared with the structural detail. In order to express the spatial variability of orientation of

streamflow direction, the drainage basin was compartmentalised into a rectilinear grid where each cell was 10 km^2 in area. In was used to calculate preferred stream-flow direction in each part of the network. Where adjacent cells showed the same patterns, these were grouped into regions; it is assumed that each region was probably conditioned by the same, unique set of controlling factors. The drainage elements oriented parallel was independently calculated for all **four** study basin Oriental data for both stream flow and structural elements was considered in respect of external segments (first order streams), internal segments (streams of second and higher orders) and jointly for streams of all orders. This was so as to examine whether or not stream order was related to geological structure. In basin area of the Denwa, the relationship of streamflow direction to fault traces and zones of mylonite was investigated. In the Denwa, Bainganga and Dudhi basin, fault traces and rock lineations are existing; and in the Nagduari basin, fault traces and the old thrust front was studied, where the structural features are not unimodel. These basins are lacking a statistically-reliable number of lineations and quantitative analysis of relationship between streamflow direction and structure is difficult at the tneso-scale.

4.1. Basin Shape

[24] Natural river basins commonly conform to a horizontal condition of self-similarity *[Peckham,* 1995; *Maritan et al.,* 1996; *Rigon et al.,* 1996; *Smith et al.,* 1997; *Veneziano and Niemann,* 2000a, 2000b; *Dodds and Rothman,* 2001]. This self-similarity considers only the properties of a basin that can be represented in the horizontal plane such as the basin boundary and the channel network. The condition states that horizontal properties of a small basin appear statistically identical to those of a large basin if the small basin is isotropically rescaled in the horizontal directions to be the same size as the large basin (Figure 4). The term "statistically identical" allows for deterministic differences in the characteristics, but it implies that the characteristics after rescaling do not reveal the original scale of the basin. This self-similarity condition is understood to apply over a limited range of scales *[Rigon et al.,* 1996]. Figure 4 illustrates this point. After rescaling, the small basin is still distinguishable from the large one because it has fewer channels. This difference is a result of the initial drainage density of the basin, which determines the finest resolution of the scaling condition *[Montgomery and Dietrich,* 1992; *Montgomery and Foufoula-Georgiou,* 1993].

[25] Various conditions have been written to describe the horizontal self-similarity of river basins *[Peckham,* 1995; *Maritan et al.,* 1996; *Veneziano and Niemann,* 2000a]. One general expression for the rescaling can be written as:

$$\zeta(L) \overset{d}{\equiv} r^{-H_n} \zeta(rL). \tag{8}$$

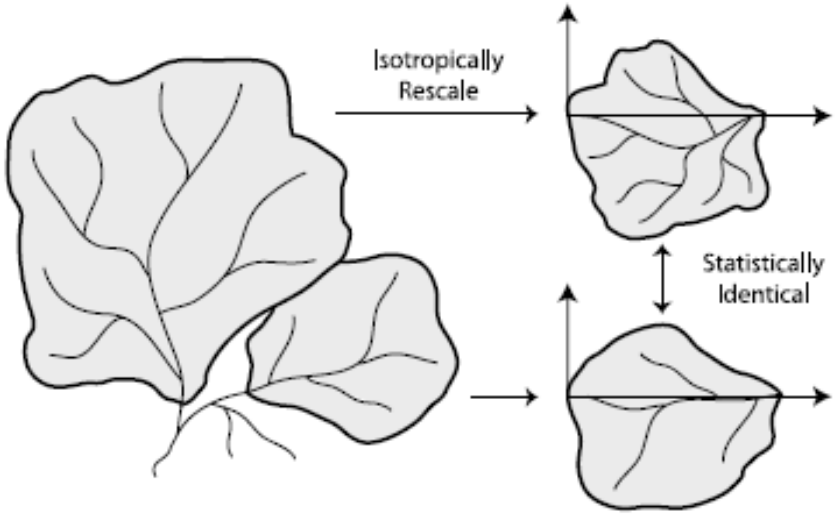

Figure 4. **Illustration of the horizontal self-similarity condition.**

where L is the Euclidean distance between the mainstream source and the basin outlet, r is a linear rescaling factor, H_h is the Hurst exponent for horizontal scaling, and ζ refers to any linear horizontal property of the basin that is measured perpendicular to L. The symbol $\overset{d}{\equiv}$ indicates that the left and right sides of the equation have the same distribution (i.e., they are statistically identical). Equation (8) can be interpreted as a comparison between two basins. The left side refers to the property ζ of a basin

with size *L*. The right side refers to the same property of a basin of size *rL*. Notice that *r* simply relates the sizes of the two basins. Equation (8) states that the property of the basin on the left side is drawn from the same probability distribution as the property of the basin on the right side if the latter is multiplied by a factor r^{-Hh}. $If\ H_h \neq 1,$, equation (8) scales the basin's longitudinal and latitudinal directions differently. In particular, the direction of L is rescaled by r^{-1}, and the direction of ζ is rescaled by r^{-Hh}. Such anisotropic scaling is called self-affinity. Most natural basins are well approximated by self-similarity, which implies that H_h is near one and the scaling is isotropic. Notice if $H_h = 1$ then the rescaling procedure is identical in all directions, so ζ can be any linear horizontal property of the basin.

[26] In any case, an acceptable choice for ζ is the width of the basin, which can be defined as the maximum extent of the basin in the direction perpendicular to *L*. If *W is* used to denote width, equation (8) can be rewritten

$$W(L) \overset{d}{=} r^{-H_n} W(rL) \tag{9}$$

This relation holds for all *L*, so *L* = 1can be choosen In that case, *r* takes on the meaning of *L,* and the equation becomes

$$W(L) \overset{d}{=} W(1) L^{H_h} \tag{10}$$

where *W*(1) is the width of a basin with a Euclidean length of one unit. Basin or drainage area *A* can be calculated as $A = cLW$ where *c* is a random coefficient that describes the shape of the basin. For example, $c = 1$ if the basin is a rectangle and $c = \pi /4$ if the basin is an ellipse. Using this relationship with equation (10), a relationship can be derived between the basin width and area:

$$W(A) \overset{d}{=} [c^{H_h}/W(1)]^{-1/(H_h+1)} A^{H_h/(H_h+1)}, \tag{11}$$

Furthermore, a relationship can be derived between the basin length and area:

$$L(A) \overset{d}{=} [cW(1)]^{-1/(H_h+1)} A^{1(H_h+1)}, \tag{12}$$

[27] Similar hypothesized relationships were examined by *Rigon et al.* [1996] for 21 basins. They obtained estimates of H_h that varied between 0.75 and 1.01 with a mean value of 0.93, which supports our contention that typical basins are well approximated by horizontal self-similarity. It should be stressed that the lengths described above are Euclidean lengths, not along-stream lengths as used in Hack's law *[Hack,* 1957]. Hack's law will be considered in more detail later in the paper.

[28] The horizontal scaling invariance of river basins provides a convenient framework to compare basins of different sizes. For example, if horizontal self-similarity holds, then $H_h = 1$ and equation (12) can be written

$$L(A) \overset{d}{=} [cW(1)]^{-1/2} A^{1/2}. \tag{13}$$

Rearranging, it can be written

$$\frac{L(A)}{A^{1/2}} \overset{d}{=} \frac{1}{[cW(1)]^{1/2}} \tag{14}$$

The right side of this equation is simply a random variable that is independent of basin scale, which implies that the left side is also independent of basin scale. Thus, if one plots the ratio of $L(A)/A^{1/2}$against *A*, one should observe a stationary random process. The mean value of this process is a measure of the typical length of a basin relative to its area or, equivalently, a normalized measure of basin elongation. Similar measures for the shapes of basins have been used previously. *Horton* [1932] suggested a measure for basin shape that is essentially, $A/L^2(A)$and *Miller* [1953], *Schumm* [1956], and *Chorley et al.* [1957] all proposed alternative measures.

[29] Figure 5 plots $L(A)/A^{1/2}$ against *A* for the four experimental runs as well as two natural basins. To generate the curves for a natural basin, the Euclidean length and drainage area are calculated at every point in the basin. The Euclidean length is calculated as the distance between each point and its mainstream source, where the mainstream is determined by selecting the tributary with the largest upstream area at every confluence.

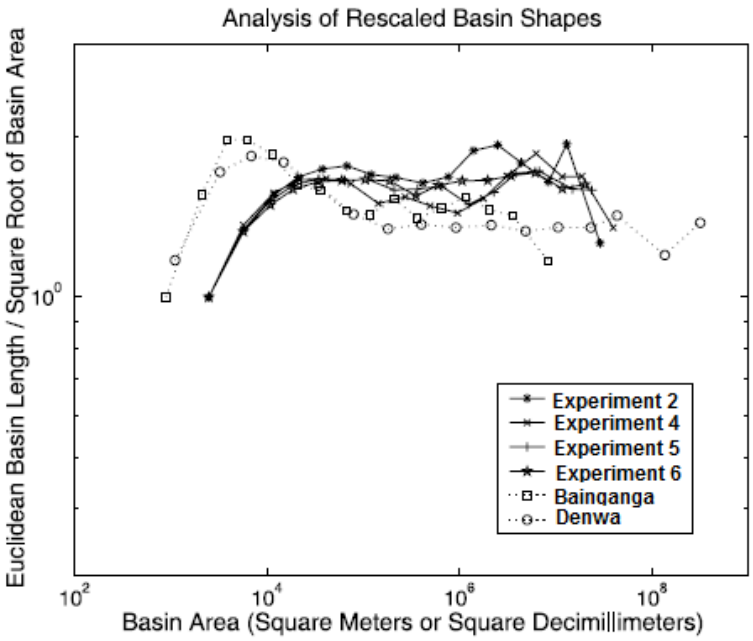

Figure 5. Comparison of the experimental basin shapes to natural basin shapes.

The results for all the points are then sorted according to basin area, and average values of length are calculated over small ranges of basin area. These averages are plotted in Figure 5. The same procedure is used for the experimental topographies, but not all points in the tank are included. In some cases, small basins form near the walls of the tank, and it is neglected that the points in these basins. In Figure 3 the neglected points are left unshaded, which accounts for the deviations from the oval shape of the tank. In Figure 5 the *y* axis is dimensionless, but the *x* axis has units of area. For the experiments, the areas have units of square decimillimeters (1 decimillimeter = 0.0001 meters). For the natural basins, the areas are in square meters. Thus the horizontal position of the results for each basin is essentially arbitrary.

[30] Considering the results for the natural basins, the elongation measure is near one for the smallest areas. The measure then increases to a maximum value and finally decreases toward a value that holds over a wide range of areas. The smallest possible basin area is a single grid cell. Because the grid cells are square, the elongation measure for the smallest basins is fixed artificially at one.

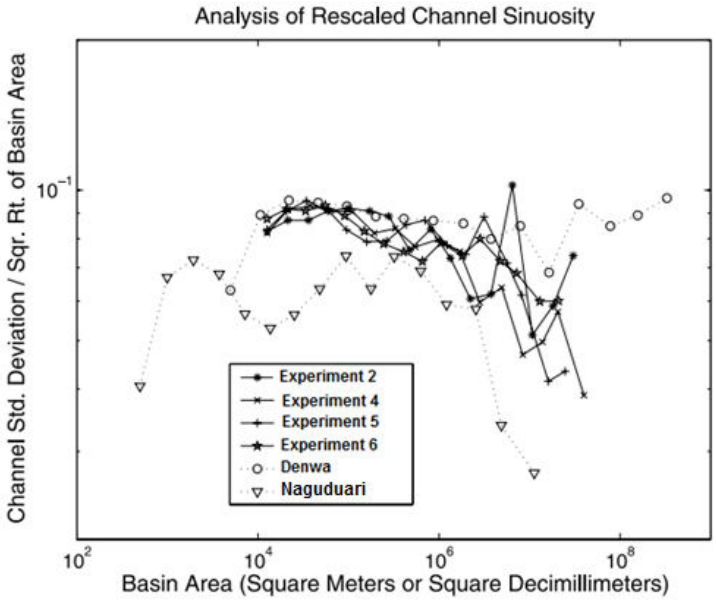

Figure 6. Comparison of the sinuosity of the experimental channels to that of natural channels.

As one considers slightly larger drained areas, the entire area is still confined to a single hillslope, which is often approximately planar. This form causes the elongation measure to grow with increasing basin area. At some point, aggregation begins to occur and the elongation measure declines. This decline corresponds to the hollows that are often found at channel heads. At the channel heads, area is accumulated from hillslopes in several directions, which reduces the elongation. As one considers points further down the channel network, the degree of elongation remains approximately constant. The constant elongation confirms that horizontal self-similarity holds for the basin shapes after one exceeds the scale of the hillslopes. While self-similarity requires the elongation measure to follow a horizontal line, it does not predict the mean value of this line. Both natural basins shown have similar values for the elongation measure in the self-similar range (approximately 1.4). For clarity, the results for the Dudhi and Nagduari basins are not shown in Figure 5. Both of these basins resemble the Bainganga basin, with elongation measures near or slightly above 1.4 in their self-similar ranges.

[31] The experimental basins produce results that resemble the natural basins. In particular, the experimental basins exhibit self-similar shapes over a range of sizes. At large areas, the elongation occasionally increases to higher-than-expected values. However, the high values occur at different areas in the different experiments, so it is interpreted them as localized variations rather than systematic changes in elongation.

[32] Figure 5 shows two significant differences between the experimental and natural basins. First, the elongation measure for experimental basins does not reach a maximum before declining to a lower value in the self-similar range. Instead, the maximum value coincides with the value in the self-similar range. This behavior suggests that the experimental basins have a subtler transition between the non-aggregating hillslopes and the aggregating values. This type of transition is confirmed by an inspection of Figures 1 and 3. In the experimental setup, the precipitation was simulated in a manner that minimized rain splash effects. Soil development are absent in the experimental landscapes. Experiments 2 and 4 exhibit moderate hillslope failure activity, but overall, surface runoff is the dominant erosive process in the physical experiments. Consequently, hillslope processes are relatively weak, and the hillslope scale is quite small. Deep hollows are occasionally observed at channel heads in the experimental topographies, but they are relatively uncommon.

[33] The second difference between the experimental and natural basins occurs in the self-similar portion of the plot. Once the curves for the experimental topographies become approximately horizontal, they stabilize at values that are above those of the natural basins (around 1.6). This difference implies that the experimental basins are slightly more elongated across a range of scales than the natural basins are considered. Interestingly, experiments with more mobile channel networks (experiments 2 and 6) do not exhibit systematically higher or lower elongation measures than experiments with more stable channel networks (experiments 4 and 5). In fact, the results from experiments 5 and 6 are nearly identical. As a result, it is concluded that the difference in the elongation of experimental and natural basins is not related to the lateral movement of channels.

4.2. Channel Sinuosity

[34] The horizontal scaling invariance condition described earlier also has implications for the sinuosity of channels. In equation (8), the horizontal characteristic ζ can be any linear measure of the basin that is measured perpendicular to L. To examine sinuosity, it is chosen ζ to be the standard deviation of the basin's mainstream measured in the direction perpendicular to L. If the standard deviation is denoted by s, equation (8) can be rewritten

$$\sigma(L) \stackrel{d}{=} r^{-H_h}\sigma(rL). \tag{15}$$

Following the same procedure that was used for basin width, it can be derived

$$\sigma(A) \stackrel{d}{=} \sigma(1)\,[cW(1)]^{-H_h/(H_h+1)}A^{H_h(H_h+1)} \tag{16}$$

where $\sigma(1)$ is the standard deviation of the mainstream of a basin with a Euclidean length of one unit. As shown in Figure 5, both the experimental and natural basin shapes are approximately self-similar. If this self-similarity holds for all horizontal properties, then $H_h = 1$ and

$$\sigma(A) \stackrel{d}{=} \sigma(1) / [cW(1)]^{1/2} A^{1/2}. \quad (17)$$

A non dimensional measure of stream course sinuosity can be derived by dividing this equation by $A^{1/2}$, which produces

$$\frac{\sigma(A)}{A^{1/2}} \stackrel{d}{=} \frac{\sigma(1)}{[cW(1)]^{1/2}}. \quad (18)$$

Notice that the right side of this expression is independent of the basin area, which confirms that the left side of this equation must also be independent of *A*. Thus a plot of $\sigma(A)/A^{1/2}$, against *A* should produce a horizontal line whose mean value reflects the typical sinuosity of the mainstream relative to the area of the basin. This measure of stream sinuosity has been used previously. *Veneziano and Niemann* [2000b] applied this measure to seven natural basins as well as the results of a numerical model. The authors found that self-similarity approximately holds for all of the cases they examined.

[35] Figure 6 plots the sinuosity measure for both the experimental and natural basins. This plot was produced in a manner similar to Figure 6. Each point was selected as the outlet of a basin, and the basin area *A* and the standard deviation of the mainstream a were measured. The standard deviation was calculated by first defining an axis that passes through the basin outlet and the mainstream source and then measuring the deviation of each grid point on the stream from this axis. The standard deviation is essentially the mean of these measured deviations. The calculated standard deviations were sorted according to the associated basin area, and mean values of *a* were calculated for small ranges of basin area. Figure 6 shows these mean values. Again, the *x* coordinates have units of square decimillimeters and square meters for the experimental and natural basins, respectively. The sinuosity measure for the Raccoon basin is approximately horizontal, which confirms the self-similarity of the mainstream course. For the Dudhi basin, self-similarity seems to hold over a range of small areas, but at larger basin sizes, the sinuosity measure decreases. Although not shown in Figure 6, the Bainganga and Dudhi basins exhibit a similar drop in their sinuosity measures. This behavior means that the largest channels in the Bainganga basin are straighter in comparison to their basin size than those of small basins. Figure 6 also shows that the two natural basins have very different values for the sinuosity measure. The Denwa channels take values around 0.09, whereas the Nagduari channels have values around 0.06. The Dudhi and Bainganga basins have values around 0.06 and 0.05, respectively. The difference In values indicates that the sinuosity measure can vary substantially between different natural basins.

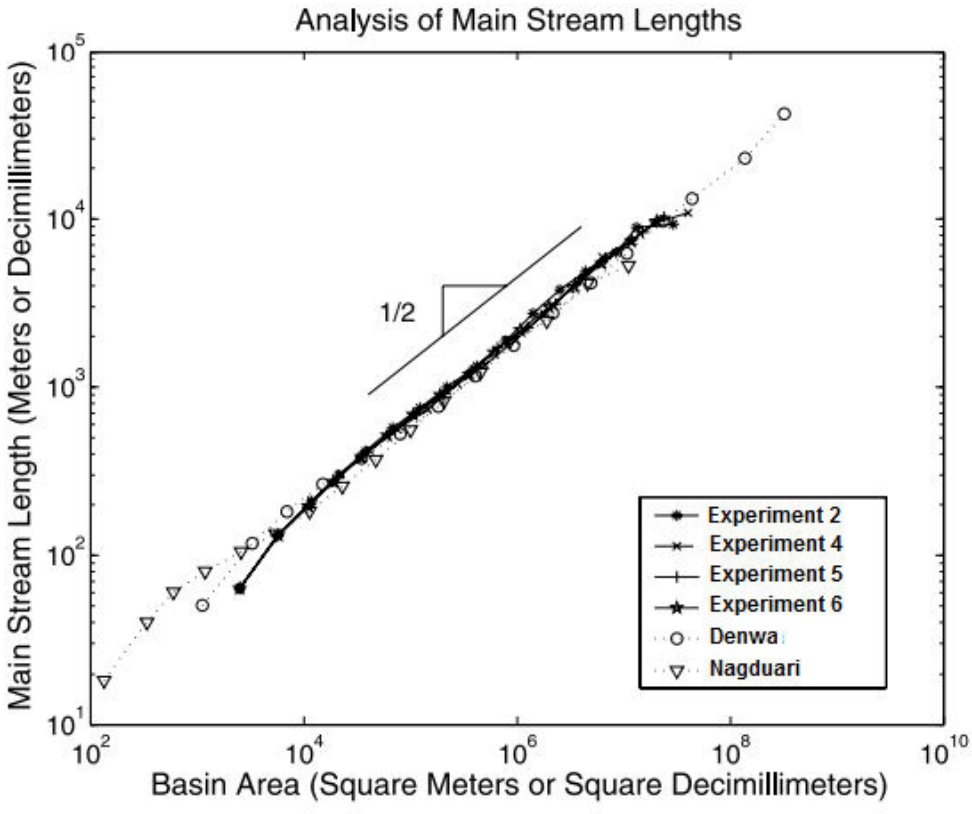

Figure 7. Hack's law for the experimental basins and two natural basins

[36] Figure 6 also shows the results for the experimental topographies. For small basin areas, the sinuosity is approximately self-similar and resembles the sinuosity of the Denwa basin. For large basin areas, the sinuosity measure decreases substantially, indicating a systematic deviation from self-similarity. One might expect that such a deviation results from the imposition of the tank boundary in the experiments. As channels approach the outlet, their sinuosity is constrained by the tank boundaries. However, the deviation from self-similarity extends down to 10^6 square decimillimeter basins. Such basins are only about 3% of the total tank area, so they often occur far from the tank outlet and boundary. It is also repeated that this analysis for a subset of basins that are far from the tank boundary in experiment 2, and we observed little difference in the sinuosity measure. Thus the decline in sinuosity is more likely a result of the erosion processes acting in the tank. It should be noted that the sinuosity measures for the different experiments are rather similar, which suggests that the degree of lateral migration of channels in the flux steady state has little impact on the sinuosity of the streams.

[37] Figure 6 indicates that the sinuosity measures for the experimental basins and the Denwa basin are similar at small areas. However, Figure 5 shows that the experimental basins are more elongated or less wide than the Denwa basin. If the standard is normalized, deviation by the basin width instead of $A^{1/2}$, the experimental basins would have higher values for their normalized sinuosity than the Denwa basin. So, the experimental channels and the Denwa channels have similar sinuosities relative to their basin areas, but the experimental channels are more sinuous relative to their basin widths.

[38] The effects of sinuosity and basin shape are both included in Hack's law, which states

$$L_m \propto A^h. \tag{19}$$

In this expression, L_m is the mainstream length, which is measured along the stream (not a Euclidean distance), and h is Hack's exponent, which is usually between 0.5 and 0.6 *[Hack,* 1957; *Rigon et al.,* 1996]. Upon initial inspection, one might expect Hack's exponent to be 0.5 for self-similar basins. In fact, Hack's exponent must be 0.5 for a self-similar basin only if the mainstream is straight. If the mainstream has self-similar sinuosity, the exponent can be above 0.5 *[Rigon et al.,* 1996; *Veneziano and Niemann,* 2000b]. Thus an exponent above 0.5 can result from basins becoming more elongated with increasing size or fractal sinuosity of streams. *Rigon et al.* [1996] examined the relative roles played by elongation and fractal sinuosity and found that fractal sinuosity usually explains most of the deviation from 0.5.

[39] Figure 7 plots Hack's law for the experimental and natural basins. In this plot, the units of length are deci-millimeters for the experimental basins and meters for the natural basins. The units of area are the respective length units squared. To create this plot, the mainstream length was measured from each selected basin outlet all the way to the basin divide, which removes the need to estimate the extent of channelization. This procedure introduces some deviation from power law scaling at small areas, but it has little effect on the behavior of Hack's law for larger basin areas. Figure 7demonstrates that Hack's law holds for the experimental topographies, and Hack's exponent is very close to 0.5. One might expect a value above 0.5 because the basin elongation does not change with increasing basin scale and the channels are sinuous. However, Figure 6 showed that the sinuosity decreases with increasing basin scale (i.e., it is not self-similar), which allows the exponent to remain near 0.5.

4.3. Slope-Area Relationship

[40] The previous analyses have focused on horizontal characteristics of the basins. It is now considered the basin topography in three dimensions. Natural basins commonly conform to a type of self-affinity, which differs from that of other surfaces because basins are not spatially homogeneous *[Veneziano and Niemann,* 2000a]. One way to express the self-affinity of basin topography is:

$$\Delta_z[L - \Delta L, L] \stackrel{d}{=} r^{-H_v}\Delta z[r(L - \Delta L), rL] \tag{20}$$

where Δ_z is the elevation difference between two points in the channel network and H_v is the Hurst exponent characterizing the vertical rescaling. The left side of equation (20) refers to an elevation difference between two points that are located at distances L - ΔL and L from their mainstream source. The right side refers to the elevation difference between another set of points, located distances $r(L - \Delta L)$ and rL from their mainstream source. In this condition, the distance L can be Euclidean distance or distance measured along the channel, as long as the along-stream distance is approximated in an appropriate manner (for more details, see *Veneziano and Niemann* [2000b]). The factor r relates the locations of the points on the left and right sides of the equations. For example, if $r > 1$, then the points on the right side of the equation are farther from their mainstream source (because $rL > L$) and farther from each other (because $r\Delta L > \Delta L$). As a whole, equation (20) states that the elevation

difference between the two closely spaced points near the basin headwaters is statistically identical to the elevation difference between two widely spaced points far from the headwaters if the latter is rescaled according to r^{-H_v}. Figure 8 illustrates this condition using only one horizontal dimension for simplicity. The illustrated case is simpler than the three-dimensional case because the distances on the left and right sides of equation (20) must refer to the same mainstream source.

[41] If the equation is divided (20) by ΔL on the left side and $r\Delta L/r$ on the right side, it is obtained:

$$\Delta_z[L-\Delta L, L]\Delta L \stackrel{d}{=} r^{1-H_v}\Delta z[r(L-\Delta L), rL]/\,(r\Delta L). \tag{21}$$

The left side is now an approximation of the channel slope at location L, where the slope is measured over a discrete upstream distance ΔL. Similarly, the right side contains an approximation for the slope at location rL, where the slope is measured over an upstream distance $r\Delta L$. It is denoted that these two slopes as $S_{\Delta L}(L)$ and $S_{r\Delta L}(rL)$, respectively, and rewrite equation (21) as

$$S_{\Delta L}(L) \stackrel{d}{=} r^{1-H_v}\ S_{r\Delta L}(rL). \tag{22}$$

If $L = 1$ os chosen, then r takes on the meaning of L, and equation (22) can be rewritten

$$S_{\Delta L}(L) \stackrel{d}{=} L^{1-H_v}\, S_{L\Delta L}(L) \tag{23}$$

where $S_{\Delta L}(1)$is the slope at a distance of one unit from the mainstream source. Equation (12) describes the scaling relationship between L and A. If this relationship is substituted for L in equation (23), it is obtained

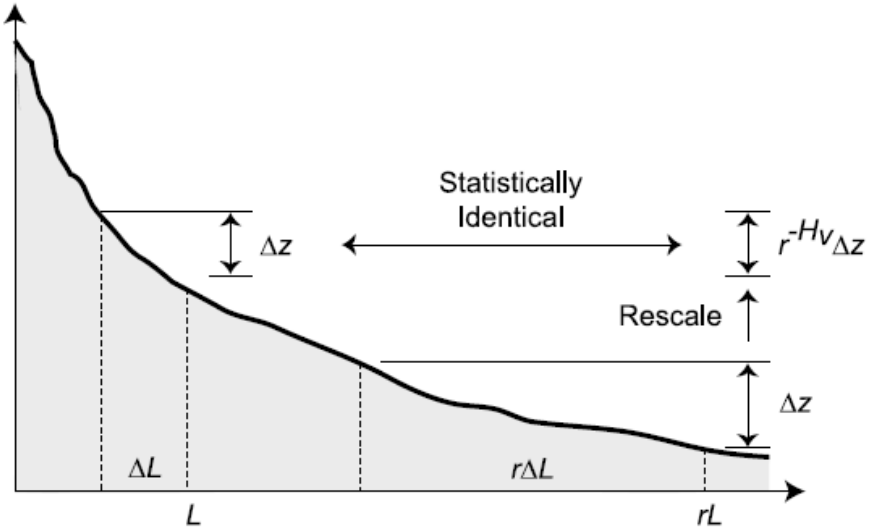

Figure 8. Illustration of the vertical self-affinity condition and its implications for the channel slope.

$$S_{\Delta L}(1) \stackrel{d}{=} \left[\frac{A}{cW(1)}\right]^{(1-H_v)(H_h+1)} S_{\left([cW\,(1)]^{-1/(H_h-1)}A^{1(H_h+1)}\right)\Delta L}\left([cW\,(1)]^{-1/(H_h-1)}A^{1(H_h+1)}\right), \tag{24}$$

and, rearranging, it is found

$$S_{[cW(1)]^{1(H_h+1)}A^{1(H_h+1)}}\Delta L^{\left([cW(1)^{-1/(H_h-1)}A^{1(H_h+1)}\right)} \stackrel{d}{=} S_{\Delta L}(1)\ \left[\frac{A}{cW(1)}\right]^{(H_v-1)(H_h+1)} \tag{25}$$

Equation (25) is a condition for the distribution as a whole, but it implies that

$$E\left[S_{kA^{1/(H_h+1)}}(A)\right] \propto A^{(H_v-1)(H_h+1)} \tag{26}$$

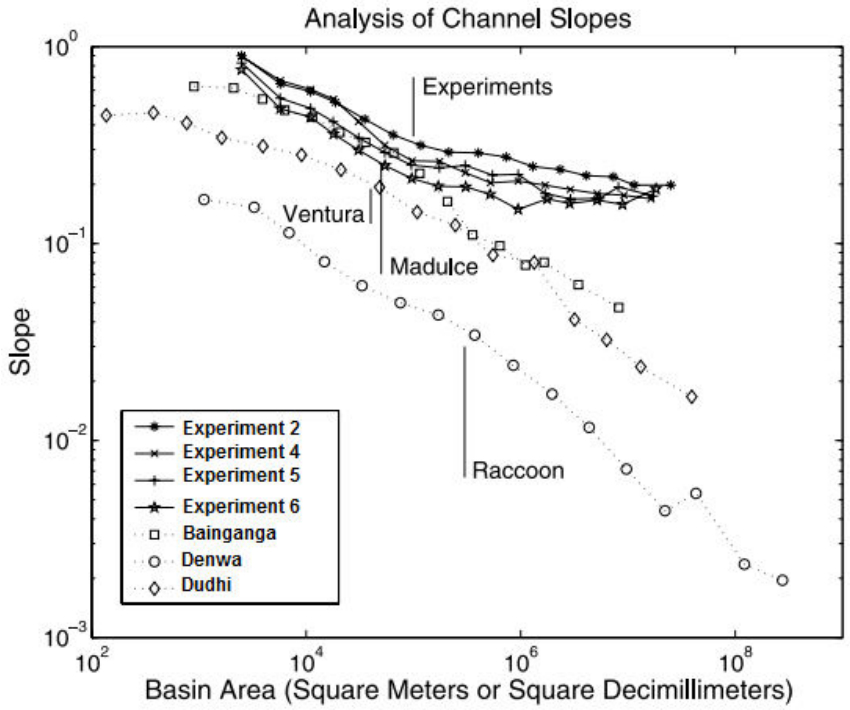

Figure 9. Relationships between mean slope and basin area for the experimental topographies and natural basins. The slopes were calculated using $k = 0.2$.

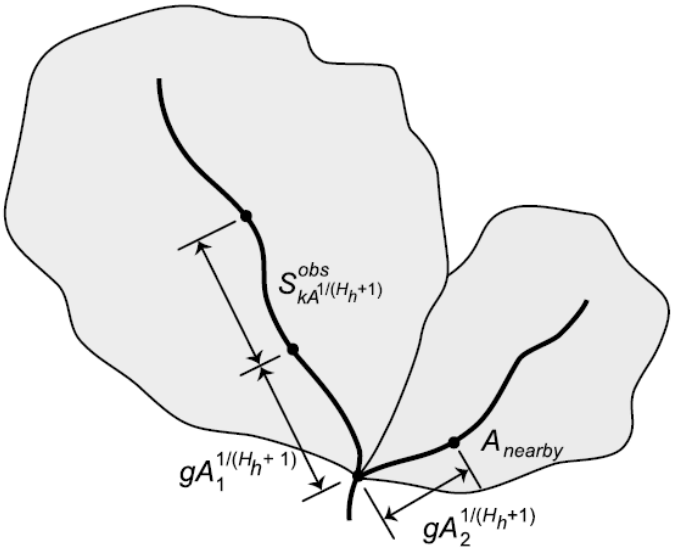

Figure 10. Conceptual framework for analyzing the variability of channel slopes and its possible dependence on nearby drainage areas.

where $E[.]$ denotes the expected value and k is any selected coefficient. Equation (26) is a form of the well-known slope-area relationship *[Flint,* 1974; *Willgoose et al.,* 1991b; *Montgomery and Foufoula-Georgiou,* 1993], and it suggests that the exponent of this law is a function of the two Hurst exponents H_h and H_γ. Previous authors have examined the connection between scaling invariance and the slope-area relationship *[Gupta and Waymire,* 1989; *Tarboton et al.,* 1989b; *Rodriguez-Iturbe and Rinaldo,* 1997]. Natural basins commonly exhibit a power law relationship between the mean slope and area over a range of areas, but scatter in such relationships is significant and deviations from a power law also frequently occur.

[42] Figure 9 plots the mean channel slope against drainage area for the experimental and natural basins. To generate Figure 9, the slopes were measured over increasing distances with increasing drainage area as specified by the subscript in equation (26) (it is selected $k = 0.2$). The slope values

displayed in Figure 9 are average values of the slopes within small ranges of drainage area. The natural basins conform to the power law predicted by equation (26), although some irregularities are observed. The Bainganga and Dudhi basins have steeper average slopes than the Denwa basin for all drained areas due to their higher relief. The experimental basins all have similar slope-area relationships, which do not conform to a single power law across the observed range of areas. For small contributing areas, a power law seems to hold with an exponent that is similar to the natural basins.

However, for large areas, that exponent no longer applies and steeper than expected slopes occur. In this range, a power law offers a reasonable approximation, but the exponents are much closer to zero. For experiments 2, 4, 5, and 6, the estimated exponents are -0.09, -0.08, -0.08, and -0.05, respectively. If the basins are considered self-similar in the horizontal direction, these exponents imply values of H_v between 0.82 and 0.90. The vertical line labeled "experiments" in the plot identifies the approximate transition between the two power laws.

[43] The dynamic origin of this break in scaling is only partially understood. One possible cause is the tank boundary, particularly near the outlet where drained areas are large. However, channel slopes are affected over nearly two orders of magnitude, which implies that the behavior occurs both near and far from the boundaries. In addition, it is repeated that this analysis using a subset of basins that are located far from the tank boundary in experiment 2. The slope-area plot for this subset of basins exhibits little difference from the relationship shown for experiment 2. Furthermore, the break in scaling is not observed at all times during the flux steady state in any given experiment. At some times, a single power law holds up to the largest observed areas. On the basis of visual inspection of the erosion dynamics it is possible that the break in the slope-area power law is related to a transition from detachment-limited conditions at small drainage areas to transport-limited conditions at large drainage areas. Temporary sediment storage is observed primarily in the larger channels, which suggests that transport capacity is limiting sediment transport and fluvial incision in these locations. The observed break in the slope-area relationship is also consistent with theoretical transitions between detachment-limited and transport-limited conditions *[Whipple and Tucker,* 2002]. However, it is also possible that the fluvial erosion process in the experiments does not have a power law dependence on drainage area.

4.4. Slope-Area Scatter

[44] Figure 9 examines only the central tendency of the slope as a function of drainage area. However, enormous scatter is observed in the slope-area plots for both the experimental and natural basins. The variability of slopes for a given area has been examined from a variety of perspectives. The scaling of the higher moments of slope with area has been examined to determine whether self-affinity or multifractality better describes the rescaling properties of natural basin topography *[Gupta and Waymire,* 1989; *Tarboton et al.,* 1989b]. The physical origin of the slope-area scatter was investigated by *Moglen and Bras* [1995a, 1995b], who introduced spatial variability into the erodibility parameter of a detachment-limited model. They found that such variability not only produces scatter in the slope-area plot, but it also modifies other scaling properties of the basin. Other results have suggested that the scatter depends on other morphological properties of the basin. *Willgoose* [1994] demonstrated that a transport-limited model in a declining equilibrium state produces a slope-area relationship with scatter that depends in part on the average elevation of the drained area.

[45] In this section, a closer look is taken at the scatter in the slope-area relationships. The experimental channel networks migrate and reorganize in the flux steady state, and such mobility is especially pronounced in experiments 2 and 6. It is hypothesized that the slope at a location depends not only on the area that currently drains through that point but also on the area that recently drained through that point. For example, a small slope might occur at a point with a small drainage area because a large channel recently occupied that location. Unfortunately, the topographic data are not available at a sufficient temporal resolution to test this hypothesis directly. In addition, no equivalent temporal data are available for the natural basins to make such a comparison. To overcome these limitations, it is noted that the experimental channels tend to move horizontally, which suggests that the drainage areas near a point likely contain information about the area that historically drained through the point.

[46] An explicit measure of the variability in the slope-area relationship is required to test this hypothesis. It is quite interesting that, in the observed slope relative to the slope expected for a point with the observed drainage area. Mathematically, this quantity is

$$\frac{S^{obs}}{E[S(A)]} \tag{27}$$

where S^{obs} is the observed slope and *E[S(A)]* is the expected value of the slope for the observed drainage area. Although the subscripts to simplify our notation is removed, the slopes must be measured over distances that depends on the local area (i.e.,$kA^{1/(H_h+1))}$) to maintain consistency with the slope-area relation in equation (26). Using equation (26), the denominator of equation (27) is proportional to the drained area to a power. Thus

$$\frac{S^{obs}}{A^{(H_v-1)/(H_h+1)}} \tag{28}$$

This ratio is essentially the coefficient in a slope-area relationship. If one writes $S = bA^{-\theta}$ where θ the empirical slope-area exponent is and b is a random variable, then one can determine the coefficient b by calculating the ratio $S/A^{-\theta}$

[47] To determine whether the ratio in equation (28) depends on morphological variables such as nearby drainage areas, the ratio can be plotted against the variables of interest and calculate whether any correlation is present. In Practice, θ must be found from the slope-area relationship before the ratio can be calculated. As Figure 8 demonstrates, the slope-area exponent holds only for a limited range of areas. Thus all the points used in this correlation analysis must have values for drainage area within the appropriate range.

[48] It is specifically interested in whether the ratio depends on nearby drainage areas, so a conceptual framework is needed that identifies an appropriate nearby area. Figure 10 illustrates the selected framework, which focuses on junctions in the channel network. One incoming tributary is used to determine the slope S^{obs} and drainage area A that are used to calculate the ratio in equation (28). The other incoming tributary is used to calculate the nearby area A_{nearby} This approach is advantageous for three reasons. First, it operates entirely on the drainage network, which helps to confine both A and A_{nearby} to the range in which the exponent 9 or equivalently $(H_v — 1)/(H_h + 1)$ applies. Second, it identifies a value of A_{nearby} that potentially impacts the observed slope. Because of the horizontal migration of channels, the channel represented by A_{nearby} may have recently occupied the location where the slope is measured. Certainly, other choices for A_{nearby} are possible. Third, this approach allows us to control the proximity of A_{nearby} to the point of interest. a specified distance. A can moved up the respective tributaries before calculating $S^{obs}A$ and A_{nearby} to operate in a manner that is consistent with the self-affinity condition, the distances should be relative to the sizes of the associated basins. Specifically, we should move up the tributaries by distances $gA_{nearby}^{1(H_h+1)}$ and $gA^{1/(H_h+1)}$, where g is a selected parameter. Other methods could be used to shift the points, but this one is consistent with the scaling properties identified previously.

[49] To use this procedure, three parameters must be specified. First, the lowest acceptable value for A and A_{nearby} to the point of interest. One can move a specified distance up the respective tributaries before c must be determined. Second, g must be selected to find the locations where A and A_{nearby} to the point of interest. A specified distance can be moved up the respective tributaries before c should be calculated. Third, k must be selected to determine the distance over which the slopes should be measured. An acceptable range of drainage areas can be found from Figure 9. The vertical line segments denote the minimum acceptable area for each basin. In all cases, these limits are conservatively identified so that a power law holds with good approximation in the range of areas analyzed. Initially, $g = 0$, so A_{nearby} is selected and measured close to the location where the slope-area coefficient (the ratio in equation (28)) is calculated. The parameter k must be small enough to ensure that the slope is measured over a distance that is in close proximity to the junction. If k is too small, then the pixel size limits the ability to calculate the slope over the appropriate distance. It is found that values of k around 0.1 to 0.2 give reasonable results.

[50] Figure 10 shows the results of this analysis for the Bainganga and Dudhi basins as well as the basins from experiments 5 and 6. The y coordinate is the coefficient in the slope-area power law, and the x coordinate is A_{nearby} /A to the point of interest. One can move a specified distance up the respective tributaries before c/A. The data for the Bainganga basin fall along a horizontal line, which indicates that the deviation of the observed slope from the expected value is not dependent on the nearby area. Although not shown in Figure 10, similar behavior is observed for the Denwa and

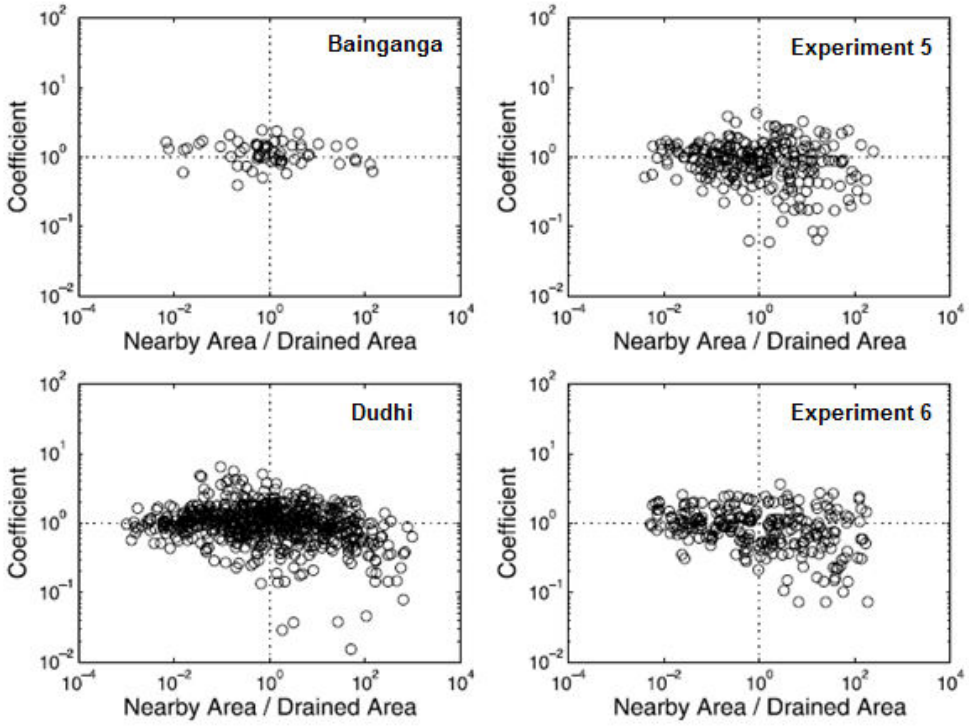

Figure 11. Plots of the ratio $S_{kA^{12}}^{obs}$ (the slope-area coefficient) where k = 0.1 and θ is taken from the slope-area relationships in Figure 8.

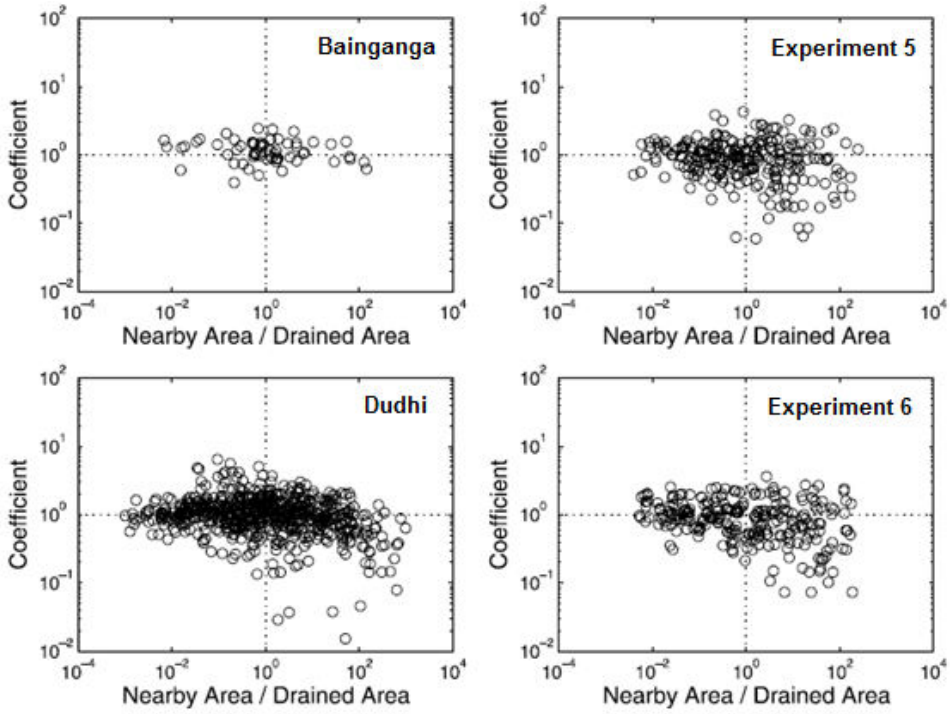

Figure 12. The same analysis as shown in Figure 11 except the slopes and areas are measured after moving a distance $gA^{1/2}$ upstream, where g = 0.2 and A is the drainage area of the tributary at the junction.

Nagdawri Bainganga basins. The plots for the Dudhi basin and experiments 5 and 6 show a different behavior. When to the point of interest, One can move a specified distance up the respective

tributaries before A_{nearby} /A < 1, the deviation is still independent of the nearby area, but when A_{nearby} /A to the point of interest. One can move a specified distance up the respective tributaries before, the observed slopes tend to be lower than the expected value. This pattern indicates that the slopes of large channels do not depend on areas of nearby small channels, but the slopesof small channels are reduced if there is a large channel nearby. Significant scatter is observed in the plots, so the nearby area does not exclusively control the deviation from the expected value of slope. In the case of the Dudhi basin, the largest channel has produced a wide valley bottom, perhaps due to horizontal channel movement associated with alluviation. Because the nearby small channels cross this valley, they have reduced slopes.

[51] For the experiments, if the observed dependence results from the mobility of the channels, then the dependence should be more pronounced for the experiments with more mobile channels. Experiments 2 and 6 had more mobile channels than experiments 4 and 5, and the observed dependencies are more significant for experiments 2 and 6. To further illustrate this observation, g is increased from 0 to 0.2, which implies that the drainage areas and slopes are calculated after shifting upstream in both tributaries. This procedure measures characteristics that are typically further apart to test the spatial scale of the observed dependence. Figure 12 shows the results when $g = 0.2$. The plot for the Bainganga basin still reveals no dependence, and the results for experiment 5 indicate very little dependence as well. The Dudhi basin still exhibits substantial dependence and some dependence is observed in experiment 6. These results confirm that more mobile channels in the experiments coincide with a stronger dependence of the slopes on nearby areas.

[52] The results in Figures 11 and 12 can also be verified visually. In Figure 3 a band of pixels is colored black to help visualize the cross-sectional shapes of the major valleys. In experiments 2 and 6, these valleys are approximately u-shaped, so smaller channels that connect to these major channels must have reduced slopes compared to those connecting to smaller streams. Experiments 4 and 5 have more v-shaped valleys, which are more consistent with most natural fluvially eroded valley shapes. The broad valley bottoms can also be seen in the photos of experiments 2 and 6 in Figure 1.

[53] These results suggest that the erosion dynamics in the experiments might differ from those occurring in many natural basins. In the cases where the channels exhibited the most mobility, the slopes of small channels located near large channels were reduced. While a similar tendency was observed in the Dudhi basin, it was not observed in the Denwa and Bainganga, basins. So it appears that most of the natural channels that examined have less horizontal mobility than the channels in the experiments. It should be stressed that no causal relationship has been demonstrated between the mobility of the channels and this morphology. The observed dependencies may in fact have other origins that are coincidental with the amount of horizontal mobility in the experiments. For example, it is possible that the discharge of the large channels is unexpectedly distributed among several grid cells instead of the single strand of points that identify as a large channel. This distribution of discharge could occur on the surface or in the subsurface. If the flow is distributed in this fashion, it would effectively augment the flow of nearby points and potentially reduce their slopes. However, based on visual observations of the discharge patterns and the spatial scales over which the slopes are measured, this cannot be believed to be the case. Alternatively, it is possible that data processing methods have artificially modified these slopes. However, this explanation seems inconsistent with the fact that the experiments with more mobile channels exhibit a stronger dependence. In the end, these results, while intriguing, cannot be considered conclusive.

[54] The observed dependence of the slopes on nearby drainage areas has another interesting implication. A slope-area relationship can be written for each tributary at a junction:

$$S_s = b_s A_s^{-\theta} \tag{29}$$

$$S_P = b_P A_s^{-\theta} \tag{30}$$

where the subscripts S and p denote the secondary and primary tributaries, respectively. The primary tributary is defined as the incoming channel with the larger drainage area. If the coefficients in equations (29) and (30) are independent of the drainage areas, The ratio of the two equations can be taken and write

$$\frac{S_S}{S_P} \propto \left[\frac{A_S}{A_P}\right]^{-\theta} \tag{31}$$

This equation states that the ratio of the tributary slopes depends on the ratio of the drained areas according to a power law with the same exponent as the basin-wide slope-area relationship (θ). Equation (31) is sometimes used to estimate the ratio of two parameters *(m/n)* in the detachment-limited erosion model *[Seidl and Dietrich,* 1994; *Niemann et al.,* 2001] because the exponent in the

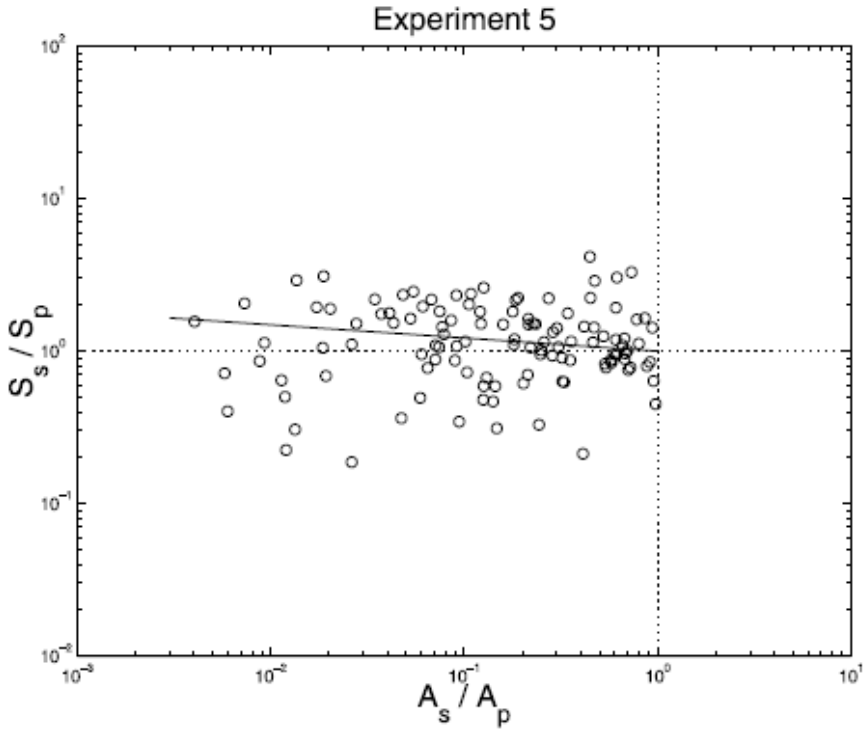

Figure 13. Plot of the ratio of tributary slopes against the ratio of tributary drainage areas (k = 0.2 and g = 0). The line indicates the trend expected from a slope-area relationship in Figure 8.

Equation can be shown to be equivalent to —*m/n*. An implicit assumption in this procedure is the independence of each tributary slope from the opposite drainage area.

[55] Figure 13 plots the ratio of the tributary slopes against the ratio of the tributary areas for experiment 5. If the slope-area coefficients were independent of the drainage areas, then the data should approximate a line in log-log with a slope that matches the exponent of the slope-area relationship in Figure 8 (within the appropriate range of drainage areas).

The line in Figure 13 indicates the trend that would match the relationship from Figure 9, and the data do not adhere to this trend. If one assumed that a detachment-limited model applied to this experimental basin and estimated the ratio of *m/n* from this procedure, the result would be spurious due to the interdependence of the slopes.

5. Conclusions

[56] In this paper, the morphology of drainage basins generated from a series of laboratory experiments was compared with that of typical natural basins. The following key observations are made.

[57] 1. All of the experimental basins had horizontal shapes that were approximately self-similar. The self-similarity implies that smaller basins within the experiments had shapes that were similar to those of larger basins. This characteristic matches the results commonly obtained for natural basins. However, the experimental basins were more elongated at all scales than the natural basins considered here.

[58] 2. The sinuosity of the main channels as measured by the lateral standard deviation of the mainstream course deviated from self-similarity. This tendency implies that larger channels in the experiments are less sinuous relative to their basin sizes than small channels. While this characteristic differs from many natural basins *[Veneziano and Niemann,* 2000b], the Bainganga and Dudhi basins analyzed here have a similar property. The magnitude of sinuosity relative to the basin size is comparable with the magnitude observed in some natural basins.

[59] 3. The slope-area relationships for the experimental basins are different than those of the natural basins considered here. In particular, a single power law usually does not hold across the entire range of drainage areas for the experimental topography. The break in scaling indicates that the vertical self-affinity commonly observed in natural basins does not hold for the experimental basins. The observed slope-area relationship can be approximated by two power laws. The one at small

drainage areas has an exponent that is similar to natural basins, but the one at large drainage areas has an exponent that is close to zero. *Lague et al.* [2003] observe slope-area exponents near zero for small experimental landscapes as well. The transition between the two power laws in our results is often gradual, and the typical drainage area at which the transition occurs varies stochastically in time. It is possible that the break occurs because of a transition from detachment-limited to transport-limited conditions. It is also possible that the fluvial incision process simply does not depend on drainage area according to a power law due to the flow conditions in the experiments.

[60] 4. Like natural basins, significant scatter is observed in the experimental slope-area relationships. Such scatter occurs despite the relatively uniform rainfall and substrate used in the experiments. Interestingly, some of the scatter is explained by a morphological property of the basin. In particular, small tributaries that flow into much larger channels tend to have slightly lower slopes than expected from their local drainage areas. This tendency is more pronounced in the experiments that have more horizontally mobile channels in the flux steady state. Among the natural basins tested, only the Dudhi basin exhibits a similar property. This tendency suggests that many natural channels might not be as mobile as the experimental ones. It is not proven that any causal relationship between this dynamic and the morphology, so this result cannot be considered conclusive. However, it provides an important opportunity for further research.

[61] 5. This study has significant implications for the use of physical experiments to study long-term basin evolution. It is shown from dynamic considerations that natural and experimental flows are crudely similar in the sense that gravity is the most important component of the force budgets followed by inertial forces. The greatest dissimilarity in force budgets exists at small scales, where viscous forces are much greater than inertial and gravity forces in experimental flows. While the experimental basins are not dynamically equivalent to natural drainage basins, the geometric similarities observed here suggest a certain robustness of landscape form to dominant forces in the flow conditions. Put simply, water flowing down slope under the influence of gravity appears to be the key dynamic condition for the development of dendritic drainage basin structures. Spatial accelerations and turbulence appear to be of secondary importance, at least at the landscape scale. This observation should encourage further development and application of experimental methods to study long-term landscape dynamics.

[62] Future work should address several key issues. First, detailed temporal and spatial data collection offers enormous potential for studying the relationships between geomorphic processes (such as hillslope failure activity and knickpoint propagation) and basin morphology, and every effort should be made to obtain high-quality topographic data from experimental landscapes. Second, average substrate grain size, grain size variability, and substrate cohesion could profoundly affect the resulting dynamics and morphology of experimental drainage basins. For instance, a stiffer material may produce detachment-limited conditions *[Whipple and Tucker,* 2002], and a broader range of grain sizes could lead to a substantial bed armoring. Third, the oscillations in sediment storage in our experiments suggest that transport-limited conditions occur. Some effort should be made to develop a dissolving substrate that provides an analog for detachment-limited conditions. Fourth, the shape of the tank may be an important issue in determining landscape morphology and dynamics at large scales. Our tank was oval, and all the flow was forced to exit the tank at a single horizontally fixed location. The effect of the boundary conditions on evolving landscapes remains unclear and warrants further investigation. Fifth, the role of flow transitions in the erosion of drainage basins is an intriguing issue. Knickpoints may arise from instabilities in transitional flows occurring in the experiments. It is also possible that erosion and transport laws for transitional and laminar flows are sufficiently different from those of fully turbulent flows that different basin geometries and dynamics result. Would fully turbulent flow prove to be more erosive? Tests of this hypothesis and its impact on long-term basin evolution would provide more insight into the role of turbulence and could lead to important considerations for future experiments, such as a minimum acceptable tank size to generate fully turbulent flows. Finally, the effects of temporal variations in runoff on river morphology remain a persistent unknown. Experimental landscapes are quite sensitive to such fluctuations, but experiments have yet to be used to study the effects of runoff variability on landscape form and stream geometry. For example, it is observed that channel incision and narrowing during an experiment that was allowed to dry out in midrun. Apparently, sediment supply from hillslopes was limited during rehydration and streams incised their beds. All of the issues raised here can be studied

in controlled laboratory conditions. Experimental basins can produce relatively good approximations of natural basin morphology, and additional experimentation would provide a rich avenue for investigating drainage basin form and dynamics.

63. **Acknowledgement:-**

I would like to thank Jeffrey D. Niemann and Leslie E. Hasbargen, as on basis of their experiments I was able to conduct same experimental setup in for this paper. I thank Shri Sunny Gaurji, Managing Director of Jaypee Group, India for providing space and outstanding support for conducting the laboratory experiments.

References

Chorley, R. J., D. E. G. Malm, and H. A. Pogorzelski (1957), A new standard for estimating drainage basin shape, Am. *J. Sci., 255,* 138-141.

Crave, A., D. Lague, P. Davy, J. Kermarrec, D. Sokoutis, L. Bodet, and R. Compagnon (2000), Analogue modeling of relief dynamics, *P ys.*Chem. *Earth, Part A,* 25(6-7), 549-553.

Czirok, A., E. Somfai, and T. Vicsek (1993), Experimental evidence for self-affine roughening in a micromodel of geomorphological evolution,*Phys. Rev. Lett, 71,* 2154-2157.

Dodds, P. S., and D. H. Rothman (2001), Geometry of river networks I: Scaling, fluctuations, and deviations, *Phys. Rev. E,* 63(1), 016115,\doi:10.1103/PhysRevE.63.016115.

Ellis, M. A., A. L. Densmore, and R. S. Anderson (1999), Development of mountainous topography in the Basin Ranges, USA, *Basin Res., 11*,21-41.

Flint, J. J. (1974), Stream gradient as a function of order, magnitude, and discharge, *Water Resour. Res.,* 10(5), 969-973.

Gupta, V. K., and E. Waymire (1989), Statistical self-similarity in river networks, *Water Resour. Res.,* 25(3), 463-476.

Hack, J. T. (1957), Studies of longitudinal stream profiles in Virginia and Maryland, *U.S. Geol. Surv. Prof Pap., 294-B,* 45-97.

Hancock, G. (1997), Experimental testing of the Siberia landscape evolution model, Ph.D. thesis, Univ. of Newcastle, Callaghan, N. S. W., Australia.

Hasbargen, L., and C. Paola (1998), Experimental tests of long term drainage basin stability, *Eos Trans. AGU, 79*(45), Fall Meet. Suppl., F366-F367.

Hasbargen, L. E., and C. Paola (2000), Landscape instability in an experimental drainage basin, *Geology, 28,* 1067-1070.

Hasbargen, L. E., and C. Paola (2003), How predictable is local erosion rate in eroding landscapes?, in *Prediction in Geomorphology, Geophys. Monogr. Ser.,* vol. 135, edited by P. R. Wilcock and R. M. Iverson,pp. 231 -239, AGU, Washington, D. C.

Horton, R. E. (1932), Drainage basin characteristics, *Eos Trans. AGU, 13,*350-361.

Howard, A. D. (1994), A detachment-limited model of drainage basinevolution, *Water Resour. Res., 30,* 2261 – 2285.

Howard, A. D., and G. Kerby (1983), Channel changes in badlands, *Geol.Soc. Am. Bull., 94,* 739-752.

Howard, A. D., M. A. Seidl, and W. E. Dietrich (1994), Modeling fluvial erosion on regional to continental scales, *J. Geophys. Res., 99,* 13,971 -13,986.

Lague, D., P. Davy, and A. Crave (2000), Estimating uplift rate and erodibility from the area-slope relationship: Examples from Brittany (France) and numerical modelling, *Phys. Chem. Earth, Part A,* 25(6-7), 543-548.

Lague, D., A. Crave, and P. Davy (2003), Laboratory experiments simulating the geomorphic response to tectonic uplift, *J. Geophys. Res.,* 108(B1), 2008, doi:10.1029/2002JB001785.

Maritan, A., A. Rinaldo, R. Rigon, A. Giacometti, and I. Rodriguez-Iturbe (1996), Scaling laws for river networks, *Phys. Rev. E,* 53(2), 1510-1515.

Miller, V. C. (1953), A quantitative geomorphic study of drainage basin characteristics in the Clinch Mountain area, Virginia and Tennessee, *Tech. Rep. 3,* Dep. of Geol., Columbia Univ., New York.

Moglen, G. E., and R. L. Bras (1995a), The effect of spatial heterogeneities on geomorphic expression in a model of basin evolution, *Water Resour. Res.,* 31(10), 2613-2631.

Moglen, G. E., and R. L. Bras (1995b), The importance of spatially heterogeneous erosivity and the cumulative area distribution within a basin evolution model, *Geomorphology, 12,* 173 -185.

Montgomery, D. R., and W. E. Dietrich (1992), Channel initiation and the problem of landscape scale, *Science, 255,* 826 -830.

Montgomery, D. R., and E. Foufoula-Georgiou (1993), Channel network source representation using digital elevation models, *Water Resour. Res.,* 29(12), 3925-3934.

Niemann, J. D., N. M. Gasparini, G. E. Tucker, and R. L. Bras (2001), A quantitative evaluation of Playfair's

law and its use in testing long-term stream erosion model, *Earth Surf Processes Landforms, 26,* 1317-1332.

Niemann Jeffrey D., Hasbargen Leslie E.(2005) A comparison of experimental and natural drainage basin morphology across a range of scales journal of geophysical research, vol. 110, f04017, doi:10.1029 /2004 jf000204,

Ouchi, S. (2002), Effects of uplift on the development of experimental erosion landform, *Geol. Soc. Am. Abstr. Programs, 34,* 129.

Ouchi, S., and M. Matsushita (1992), Measurement of self affinity on surfaces as a trial application of fractal geometry to landform analysis, *Geomorphology, 5,* 115 -130.

Paola Chris, Straub Kylen Mohrig David, Reinhardt Liam (2009) the "unreasonable effectiveness" of Strati graphic and geomorphic experiments Earth-Science Reviews.2009,1-43

Parker, R. S. (1977), Experimental study of basin evolution and its hydro-logic implications, Ph.D. thesis, Colo. State Univ., Fort Collins.

Peakall, J., P. J. Ashworth, and J. L. Best (1996), Physical modelling in fluvial geomorphology: Principles, applications and unresolved issues, in *The Scientific Nature of Geomorphology: Proceedings of the 27th Binghamton Symposium in Geomorphology,* edited by B. L. Rhoads and C. E. Thorn, pp. 221 - 253, John Wiley, Hoboken, N. J.

Peckham, S. D. (1995), New results for self-similar trees with applications to river networks, *Water Resour. Res.,* 31(4), 1023-1029.

Rodriguez-Iturbe, I., and A. Rinaldo (1997), *Fractal River Basins: Chance and Self-Organization,* 547 pp., Cambridge Univ. Press, New York.

Schumm, S. A. (1956), The evolution of drainage systems and slopes in badlands at Perth Amboy, *Bull. Am. Geol. Soc., 67*(5), 597-646.

Schumm, S. A., and R. S. Parker (1973), Implications of complex response of drainage systems for Quaternary alluvial stratigraphy, *Nat. Phys. Sci.,243,* 99-100.

Seidl, M. A., and W. E. Dietrich (1994), Longitudinal profile development into bedrock: An analysis ofHawaiian channels, *J. Geol., 102,* 457-474.

Smith, T. R., B. Birnir, and G. E. Merchant (1997), Towards and elementary theory of drainage basin evolution, I, The theoretical basis, *Comput. Geosci., 23*(8), 811 -822.

Sacramento. Tarboton, D. R., R. L. Bras, and I. Rodriguez-Iturbe (1989a), The analysis of river basins and channel networks using digital terrain data, *Tech. Rep.326,*

Ralph M. Parsons Lab., Mass. Inst. of Technol., Cambridge. Tarboton, D. G., R. L. Bras, and I. Rodriguez-Iturbe (1989b), Scaling and elevation in river networks, *Water Resour. Res.* , *25*(9), 2037 - 2051.

Veneziano, D., and J. D. Niemann (2000a), Self-similarity and multifrac-tality of fluvial erosion topography: 1. Mathematical conditions and physical origin, *Water Resour. Res., 36*(7), 1923-1936.

Whipple, K., and G. Tucker (2002), Implications of sediment-flux-dependent river incision models for landscape evolution, *J. Geophys.Res., 107*(B2), 2039, doi:10.1029/2000JB000044.

Willgoose, G. (1994), A physical explanation for an observed area-slope- elevation relationship for catchments with declining relief, *Water Resour. Res.,* 30(2), 151-159.

Willgoose, G., R. L. Bras, and I. Rodriguez-Iturbe (1991a), A coupled channel network growth and hillslope evolution model: 1. Theory, *WaterResour. Res.,* 27(7), 1671-1684.

Willgoose, G., R. L. Bras, and I. Rodriguez-Iturbe (1991b), A physical explanation of an observed link area-slope relationship, *Water Resour. Res., 27*(7), 1697-1702.